Research Paper

GEOSPHERE

GEOSPHERE, v. 16, no. 1

https://doi.org/10.1130/GES02158.1

10 figures; 4 tables; 1 set of supplemental files

CORRESPONDENCE: cjones@colorado.edu

CITATION: Ryan, J., Frassetto, A.M., Hurd, O., Jones, C.H., Unruh, J., Zandt, G., Gilbert, H., and Owens, T.J., 2020, Unusually deep earthquakes in the central Sierra Nevada (California, USA): Foundering ultramafic lithosphere?: Geosphere, v. 16, no. 1, p. 357–377, https://doi.org/10.1130/GES02058.1.

Science Editor: Andrea Hampel
Associate Editor: Huaiyu Yuan

Received 21 May 2019
Revision received 14 August 2019
Accepted 19 November 2019

Published online 23 December 2019

Unusually deep earthquakes in the central Sierra Nevada (California, USA): Foundering ultramafic lithosphere?

Jamie Ryan[1], Andrew M. Frassetto[1,2], Owen Hurd[1,3], Craig H. Jones[4], Jeffrey Unruh[5], George Zandt[1], Hersh Gilbert[6], and Thomas J. Owens[7]

[1]Department of Geosciences, University of Arizona, Gould-Simpson Building #77, 1040 E 4th Street, Tucson, Arizona 85721, USA
[2]Incorporated Research Institutions for Seismology, 1200 New York Avenue NW, Suite 400, Washington, D.C., 20005, USA
[3]EOG Resources, 1111 Bagby, Sky Lobby 2, PO Box 4362, Houston, Texas 77210, USA
[4]Department of Geological Sciences and Cooperative Institute for Research in Environmental Sciences, University of Colorado, Campus Box 399, 2200 Colorado Avenue, Boulder, Colorado 80309-0399, USA
[5]Lettis Consultants International, Inc., 1981 North Broadway, Suite 330, Walnut Creek, California 94596, USA
[6]Department of Geoscience, University of Calgary, 2500 University Drive NW, Calgary, Alberta, T2N 1N4, Canada
[7]Department of Geological Sciences, University of South Carolina, 701 Sumter Street, EWS 617, Columbia, South Carolina 29208, USA

ABSTRACT

Using a network of temporarily deployed broadband seismometers, we characterize an unusual region of crustal earthquakes in the west-central Sierra Nevada, California (USA). We locate 131 earthquakes, which occurred from 3.1 to 47.1 km deep during June 2005 to May 2006. We detect more events, at greater depths, than are present in the Northern California Seismic Network catalog during this period. Most of the events occur at depths of 20–35 km and cluster into two distinct groups. In addition, some of the events appear to be repeating due to the similarity of their waveforms and locations. We calculate focal mechanisms for 52 of these events, and about half exhibit reverse faulting, which represents a state of horizontal compressional stress that is distinct from the regional stress field. From first arrivals, we calculate a one-dimensional model of crustal P-wavespeeds, which resolves a gradational increase from 5.8 km/s near the surface to 6.7 km/s at 35 km depth. The events overlie a significant variation in the character of the Moho, and two long-period events occur near the seismically imaged Moho at nearly 40 km depth. We suggest that these earthquakes could be the seismogenic response of the crust to active foundering of mafic-ultramafic lithosphere and resultant asthenospheric upwelling beneath the central Sierra Nevada.

INTRODUCTION

Deep intraplate earthquakes occur within the lower crust and upper mantle of the western United States (Wong and Chapman, 1990) in areas with a wide range of geologic and tectonic histories, including multiple regions within the Colorado Plateau, near zones of Sevier-Laramide deformation in the Rocky Mountains and Wyoming craton (Frohlich et al., 2014; O'Rourke et al., 2016), and across a plate boundary system in California. Much of this seismicity is located below 20 km depth and coincides with areas of locally low heat flow, which is indicative of temperatures low enough to allow for brittle deformation at unusually great depths (Wong and Chapman, 1990). In the eastern San Joaquin Valley and western Sierra Nevada foothills of central California, small ($M_L \leq 3.2$) earthquakes are found to ~40 km depth (Wong and Savage, 1983; Miller and Mooney, 1994). These events have been inferred to occur on crustal faults but appear to be unrelated to tectonically active features at the surface, and their cause has been heretofore unknown.

The Sierra Nevada EarthScope Project (SNEP) (Owens et al., 2005) consisted of an array of three-component broadband seismometers with a north-south extent of >400 km north from about Fresno, California, and a west-east extent of >150 km from the Great Valley to the Basin and Range (Fig. 1). The primary purpose of the SNEP was to image the deep structure of the Sierra Nevada batholith in order to better characterize the location and disposition of mafic and ultramafic lower crust and upper mantle beneath the Sierra Nevada. This root is inferred to be gravitationally unstable within the surrounding lithosphere and foundering in places beneath the Sierra Nevada (Ducea and Saleeby, 1996, 1998b; Jones et al., 2004; Zandt, 2003), a process typified by the "Isabella anomaly," which is evident in regional seismic tomography (Benz and Zandt, 1993; Biasi and Humphreys, 1992; Jones et al., 1994). The uniform spacing (~25 km) of the SNEP stations, when combined with the larger framework of the EarthScope Transportable Array (TA) and permanent regional monitoring stations, provides the opportunity to study the unusual earthquakes of the western Sierra Nevada in a manner not previously possible. Here we evaluate this seismicity and explore its potential causes.

GEOLOGIC, TECTONIC, AND GEOPHYSICAL OVERVIEW

The Sierra Nevada consists primarily of metamorphic and plutonic rocks that separate the Great Valley forearc basin on its western edge from the Basin and Range extensional domain to its east (e.g., Bateman and Wahrhaftig, 1966). Its crust records Paleozoic- to Mesozoic-age terrane accretion and batholith-producing crustal melting as subduction of the Farallon plate fueled an extensive Cordilleran arc (e.g., Ducea, 2001; Dickinson, 2008), with most of the batholith being emplaced by 85 Ma (e.g., Ducea, 2001). Subduction-related volcanism reemerged during the Miocene between present-day Yosemite National Park and Lake Tahoe (Busby and Putirka, 2009; Cousens et al., 2008). Small volumes

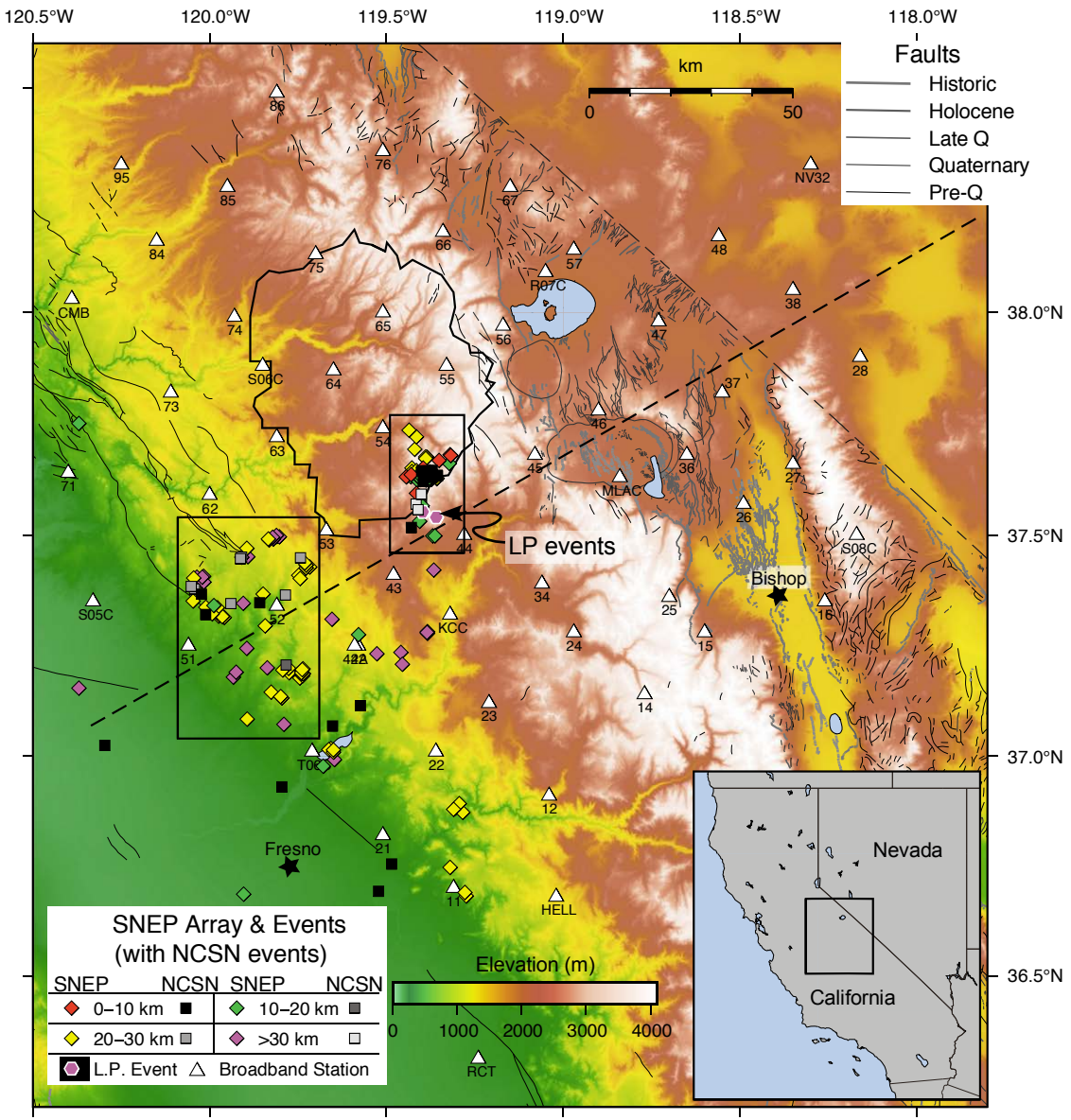

Figure 1. Map of study area with seismic stations (triangles) and earthquake locations, central Sierra Nevada, USA, including 28 events in the Northern California Seismic Network (NCSN) catalog not detected by the Sierra Nevada EarthScope Project (SNEP) and two long-period (LP) events originally identified by the NCSN. Event symbols reflect hypocenter depths and catalog of origin. The southwestern box outlines the Foothills cluster of earthquakes and the northwestern box is the Yosemite cluster. Dashed line marks the location of Figure 10. Events detected by this study are shown as diamonds and listed in Table 2, while NCSN events detected for the same time period are shown as squares. Numbered stations are from the SNEP deployment; the complete station name includes the prefix SNP. Map of the complete SNEP deployment may be viewed at https://ds.iris.edu/gmap/#network=XE&starttime=2005-01-01&endtime=2007-12-31&planet=earth. Faults shown are from Jennings and Bryant (2010) (Q–Quaternary).

of magmas began to erupt across the southern and central Sierra Nevada beginning ca. 12 Ma (Manley et al., 2000; Moore and Dodge, 1980; Dodge and Moore, 1981). Xenoliths in the oldest phase of these eruptions record near-Moho eclogitic garnet- and pyroxene-rich material present as recently as 10–8 Ma beneath the central Sierra Nevada batholith (Ducea and Saleeby, 1996). This mafic-ultramafic material, often termed arclogite, dates contemporaneously with the overlying felsic plutons and represents an unusually dense (~3500 kg/m^3) root of complimentary residue and cumulates left over by the extraction of felsic melt (Ducea and Saleeby, 1998a; Lee et al., 2001).

The cessation of subduction beneath southwestern North America, opening of a slab window, and establishment of a transform boundary (e.g., Dickinson, 1979) appear to have significantly affected the Sierra Nevada during the mid- to late Tertiary. The Sierra Nevada block experienced normal faulting on its eastern margin, which has commonly been associated with uplift and, in the central and northern Sierra, westward tilting (Christensen, 1966), though the timing of Sierran uplift remains disputed (e.g., House et al., 1998; Mulch et al., 2006). The subsequent eruption of more typical, asthenospheric spinel peridotite mantle xenoliths in the eastern Sierra Nevada suggests that the dense root foundered and was replaced beneath parts of the range between ca. 10 and 3 Ma (Ducea and Saleeby, 1996, 1998b). Evidence for uplift in the southern Sierra Nevada and an increase in extensional strain rates in the adjacent Basin and Range ca. 3.5 Ma indicates ongoing detachment during this period. Volcanism in the eastern Sierra (e.g., Long Valley caldera) may result from the subsequent inflow of asthenosphere to replace the foundered material (Jones et al., 2004).

Any lingering arclogite and old mantle lithosphere would manifest as high-wavespeed upper mantle in tomography results (Gilbert et al., 2012; Jones et al., 2014) and in receiver functions, which clearly show that the crust-mantle boundary (Mohorovičić discontinuity or Moho) deepens and becomes much less distinct west from the high Sierra Nevada toward the Sierra foothills and Central Valley (Zandt et al., 2004; Frassetto et al., 2011). A westward increase in crustal wavespeeds reduces the wavespeed contrast across the Moho, making it difficult to resolve (Frassetto et al., 2011). The region where the dense residuum still resides appears to be limited to the western portion of the Sierra Nevada south of Lake Tahoe (Frassetto et al., 2011; Gilbert et al., 2012). These western Sierra foothills have experienced both Quaternary subsidence to the south (Saleeby and Foster, 2004; Sousa et al., 2017) and uplift to the north (Jones et al., 2014; Saleeby et al., 2013).

DATA ANALYSIS AND OBSERVATIONS

Our data from the SNEP array focus on the first year of deployment between the springs of 2005 and 2006, when SNEP stations were in the vicinity of the events of interest. We used waveforms from 46 broadband seismometers recording continuously at 40 samples per second (sps) (Owens et al., 2005). SNEP data are archived at the IRIS Data Management Center (https://ds.iris.edu/ds/nodes/dmc/). The stations used extended from Fresno to just north of Yosemite National Park (Fig. 1; Table 1). Three of the backcountry stations within the SNEP array (SNP14, SNP65, SNP75) recorded at 20 sps during part or all of their deployment. Data from other temporary and permanent stations in the region were also included in our analysis. We ran a STA/LTA (ratio of short-term signal average to long-term average to identify seismic arrival) event detector in the Antelope software package (Boulder Real Time Technologies; http://www.brtt.com/software.html) to identify potential events. Although the SNEP array recorded extensive seismicity within the Owens Valley and Long Valley caldera regions, in this paper we focus on the less-well-understood events located in the western portions of the SNEP array. P- and S-wave arrivals detected and quality checked in Antelope were manually picked in SAC (Seismic Analysis Code; https://ds.iris.edu/ds/nodes/dmc/software/downloads/sac/) from vertical (P) and horizontal (S) seismograms high-pass filtered above 5 Hz. Initial locations were derived from these picks using HYPOCENTER software (Lienert and Havskov, 1995) and a five-layer wavespeed model adapted from Miller and Mooney (1994; Fig. 2, blue line).

Only earthquakes with clear body waves at no less than five stations and S-P times of 10 s or less were analyzed. Events typically had a 3–5 s S-P time at the nearest station. Including arrival times of S-waves together with those of P-waves greatly reduced the uncertainty of hypocenter locations (Gomberg et al., 1990). Locations showed little improvement by adding arrival times from stations that were more distant than the nearest five stations. Most events were small and could only be reliably picked at an average of 12 stations at distances within ~75 km of the events; only six were recorded on >30 stations including distances >150 km from the event.

We used the one-dimensional (1-D) hypocenter and wavespeed inversion program VELEST (Kissling et al., 1994) to derive a series of models from the earthquake arrival times (Fig. 2). During this process, P- and S-arrival picks were further refined, and the events were relocated with HYPOCENTER software using the preferred VELEST model discussed below. Focal mechanism solutions were calculated from P- and S-wave arrivals using FOCMEC (Snoke, 2003) run within SEISAN software (Havskov and Ottemöller, 1999).

Crustal Wavespeed

The station coverage from the SNEP deployment improves upon the few permanent seismometers and less dense TA deployment in the Sierra Nevada, thus providing the opportunity to use local earthquake arrivals to derive models of crustal wavespeed over a broader region of the Sierra Nevada than has been previously studied (e.g., Miller and Mooney, 1994). After discarding events with azimuthal gaps >180° and root mean square (RMS) travel-time residuals >1 s, we used 1225 arrival times from a total of 92 earthquakes to derive a 1-D wavespeed model using VELEST (Kissling et al., 1994). The HYPOCENTER-located events used in the inversion range from depths of 3.1–47.4 km and lie in the vicinity of the two main earthquake clusters (Foothills and Yosemite clusters; described in more detail below). In order to maintain a broad depth distribution of earthquakes, we did not attempt to create separate models for each cluster.

TABLE 1. SEISMIC STATIONS USED IN THIS STUDY

Network code	Station name	Latitude (°N)	Longitude (°W)	Elevation (m)	Station correction (s)	Number of earthquakes picked
XE	SNP11	36.699	119.312	146	–0.19	71
XE	SNP12	36.913	119.040	1284	0.05	31
XE	SNP14	37.140	118.774	3056	*	20
XE	SNP15	37.278	118.599	2434	0.14	10
XE	SNP16	37.350	118.255	1898	0.29	11
XE	SNP21	36.820	119.513	208	–0.02	87
XE	SNP22	37.011	119.360	1207	0.18	70
XE	SNP23	37.123	119.214	2087	0.05	94
XE	SNP24	37.280	118.973	2263	–0.11	10
XE	SNP25	37.359	118.705	2466	–0.02	21
XE	SNP26	37.572	118.488	1680	0.46	7
XE	SNP27	37.660	118.352	1721	0	2
XE	SNP28	37.896	118.157	1641	0	3
XE	SNP34	37.392	119.063	614	0.27	31
XE	SNP36	37.683	118.647	2457	0.49	8
XE	SNP37	37.817	118.546	1939	0.34	11
XE	SNP38	38.051	118.353	2063	0	3
XE	SNP42	37.246	119.578	942	0.1	40
XE	SNP43	37.413	119.485	2274	0.04	55
XE	SNP44	37.500	119.279	2070	0	78
XE	SNP45	37.683	119.083	2354	–0.07	29
XE	SNP46	37.783	118.902	2751	0.49	19
XE	SNP47	37.980	118.729	2074	0	3
XE	SNP48	38.169	118.559	1838	0.15	6
XE	SNP51	37.253	120.058	250	0.03	99
XE	SNP52	37.343	119.815	341	0.05	112
XE	SNP53	37.514	119.675	1472	0.01	83
XE	SNP54	37.737	119.513	1045	–0.14	69
XE	SNP55	37.880	119.333	1410	–0.15	51
XE	SNP56	37.974	119.169	2943	–0.16	33
XE	SNP57	38.143	118.967	2040	0.19	11
XE	SNP62	37.588	120.005	642	–0.22	103
XE	SNP63	37.729	119.807	1797	–0.28	15
XE	SNP64	37.843	119.647	2430	–0.12	27
XE	SNP65	38.000	119.511	2918	*	16
XE	SNP66	38.180	119.341	2429	–0.26	39
XE	SNP67	38.283	119.148	2277	0.02	48
XE	SNP71	37.642	120.404	132	–0.21	41
XE	SNP73	37.823	120.112	971	–0.35	72
XE	SNP74	37.985	119.932	1684	–0.56	16
XE	SNP75	38.128	119.697	2665	*	12
XE	SNP76	38.362	119.514	2106	–0.19	7
XE	SNP84	38.156	120.147	1610	–0.47	9
XE	SNP85	38.285	119.954	2003	–0.56	21
XE	SNP86	38.493	119.807	2632	–0.43	20
XE	SNP95	38.333	120.253	1754	–0.71	12

(*continued*)

TABLE 1. SEISMIC STATIONS USED IN THIS STUDY (*continued*)

Network code	Station name	Latitude (°N)	Longitude (°W)	Elevation (m)	Station correction (s)	Number of earthquakes picked
Non-SNEP stations						
BK	CMB	38.035	120.386	697	*	11
BK	KCC	37.324	119.319	888	*	7
CI	MLAC	37.630	118.836	2162	*	1
IM	NV32	38.334	118.299	1829	*	1
CI	RCT	36.305	119.244	107	*	1
BK	HELL	36.680	119.023	1145	*	33
TA	P05C	39.303	120.608	1756	*	1
TA	R07C	38.089	119.047	1996	*	4
CI	RCT	36.3052	119.2438	107	*	1
TA	S04C	37.505	121.328	310	*	2
TA	S05C	37.346	120.330	85	*	30
TA	S06C	37.882	119.849	1377	*	46
TA	S08C	37.499	118.171	3087	*	7
CI	SPG	36.1355	118.811	314	*	2
TA	T05C	36.895	120.674	46	*	1
TA	T06C	37.007	119.709	216	*	14
TA	U04C	36.363	120.783	813	*	3

*Stations not used in making the velocity models.

Network code abbreviations: XE—temporary deployment code used in this time period for Sierra Nevada EarthScope Project (SNEP); BK—Northern California Seismic Network (Berkeley); CI—Caltech (Southern California Seismic Network); TA—Transportable Array; IM—international miscellaneous.

Note: Station correction is a correction subtracted from the arrival time for each pick to adjust for conditions local to the station.

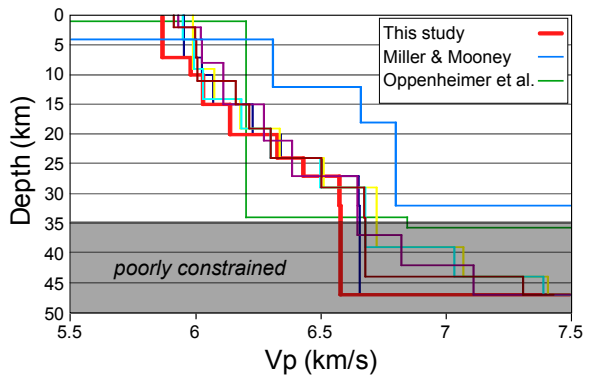

Figure 2. P-wavespeed versus depth for VELEST models (Table 3; preferred model in red; thin lines represent the suite of inversion solutions). Northern California Seismic Network (NCSN) model (Oppenheimer et al., 1993) is shown in green and the Miller and Mooney (1994) model is shown in blue. Note that models tend to scatter at depths with sparse earthquake sampling; see Figure 4. Depth of 0 km indicates sea level.

The initial VELEST inversion started from the Miller and Mooney (1994) crustal model extended with additional layers down to 50 km. After five iterations for P- and S-wavespeeds, the output model was used to derive 15 new models by perturbing the P- and S-wavespeeds. Next, each of the 15 models was run through five inversion iterations for P- and S-wavespeeds, and six models were selected from the 15 based on high values in their resolution matrix, low standard deviations associated with calculation of model parameters, and low overall RMS residuals. Finally, the six models were each run through two final VELEST iterations inverting for P-wavespeeds only (with a constant Vp/Vs ratio of 1.73) and using output of the previous run as input for the next iteration. We derived Vp/Vs from Wadati diagrams generated with first-arrival picks from the deepest events (Wadati, 1933; Frassetto et al., 2011). Due to sampling limitations, we did not independently invert for S-wavespeeds. S-wave picks are down-weighted relative to the P-wave picks for all VELEST inversions, and the six models show only slight variations between the final P- and S-wave inversions and the final P-wave-only inversions. While each of the six models exhibit distinct differences, they converge on a similar wavespeed structure following the final VELEST iterations (Fig. 2).

The final models reveal a gradational increase of wavespeed with depth. In most of the models, wavespeeds in the upper 10 km of the crust range from 5.8 to 6.1 km/s. A smooth transition from 6.1 km/s to 6.7 km/s exists from 10 km to ~35 km, while a larger transition from 6.7 km/s to 7.6 km/s is observed at lower crustal depths. For a majority of well-resolved layers, the diagonal values of the resolution matrix of the models exceed 0.8. Layers at depths >32 km are less well resolved due to only seven earthquakes (35 rays) sampling below this depth. This lack of resolution is also reflected in the large differences in wavespeeds for the six models below ~35 km (Fig. 2). Wavespeeds of the models presented here are as much as 0.5 km/s lower than that of the model of Miller and Mooney (1994). This difference likely results from our sampling including a larger portion of the granitic batholith, while the earlier model sampled more mafic material that underlies the eastern Great Valley and the Foothills metamorphic belt.

Station delays for most of the six models of crustal wavespeed, which were solved for simultaneously during inversion iterations, range from –0.71 to 0.49 s (Table 1). This broad range is unsurprising given that the SNEP array spans geologically heterogeneous sections of the San Joaquin Valley, Foothills metamorphic belt, and Sierra Nevada batholith. Overall RMS values from final models decreased from ~0.50 s in the initial iteration to ~0.15 s in the final iteration, while the average P-wavespeed model standard deviation also decreased. Epicenters shifted minimally between the initial HYPOCENTER location and the relocation with our preferred model, although depths deepened by an average of 3.2 km across all events after the relocation.

Event Waveforms and Spectra

Earthquake waveforms and corresponding spectra demonstrate the general characteristics of these events across the central Sierra Nevada. We used the GISMO data-analysis toolbox (Thompson and Reyes, 2018) for time-series processing and display; each vertical component seismogram was demeaned and detrended, then high-pass filtered (two passes, two poles) with a 0.5 Hz Butterworth filter to remove microseismic noise. Spectrograms were calculated using a fast Fourier transform length of 3 s with 1.5 s of overlap. Instrument response is flat within the displayed frequency range, and we applied a sensitivity correction to show time-series units as velocity (μm/s). Examples from different stations for each event are displayed over a common time frame starting shortly before the P-arrival (Fig. 3).

For events of all depths in the Foothills and Yosemite clusters, the arrivals of P- and S-waves are clearly observed at adjacent stations. These waveforms stand out over any remaining background noise and have consistent durations of 15–20 s at up to 30 km distance. The spectra of these earthquakes are especially prominent between 5 and 15 Hz, peaking in most cases at >70 dB above the ambient noise level (Figs. 3A and 3B). Observed variations may result from different levels of attenuation along travel paths or the azimuth of the station relative to the source mechanism.

In addition, we observe notably different waveform and spectra for two long-period event sequences. Deep long-period (LP) earthquakes have been observed at the southern edge of the Yosemite cluster (Pitt et al., 2002), and the Northern California Seismic Network (NCSN) (NCEDC, 2014) reported LP events on 14 September 2005 and 20 October 2005. These events exhibit positive, emergent P- and S-phase arrivals and plainly lower-frequency content. The first event has a 30–35-s-long waveform and may represent the comingling of several sources (Fig. 3C). The second is two-minute-long sequence that clearly delineates into distinct earthquakes (Fig. 3D), resembling the spasmodic earthquakes seen in the Long Valley caldera to the east (Ryall and Ryall, 1983). The NCSN cataloged these as two crustal earthquakes and two LP earthquakes. However, in all cases, the spectra are almost entirely lacking in energy above 10 Hz, and the signals concentrate between 1 and 6 Hz. These earthquakes were not widely viewed across the SNEP array, but one from each sequence was identifiable at enough surrounding stations to relocate.

Earthquake Locations

During the first phase of the SNEP deployment (May 2005–June 2006), we detected and located 129 earthquakes at depths between 3.1 and 47.4 km (Table 2; see also Supplemental Material[1]). Of these, 88 earthquakes were between 20 and 35 km depth (Fig. 4A). We observe no temporal pattern in the events, which occurred at a rate of 8–17 per month, but most events were part of two distinct spatial clusters. The Foothills cluster straddles the boundary between the Great Valley and the western foothills of the Sierra Nevada north of Fresno and southwest of Yosemite National Park (Fig. 1). This group includes 56 events, nearly all of which occur at depths >20 km with an average depth of 28.9 km. The other group of events straddles the southeastern boundary of Yosemite National Park, and the 48 events in this Yosemite cluster

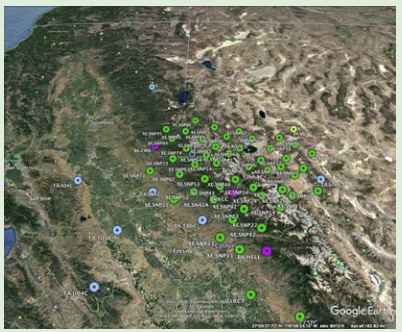

[1]Supplemental Material. ASCII text file with arrival time picks in SEISAN format. Please visit https://doi.org/10.1130/GES02158.S1 or access the full-text article on www.gsapubs.org to view the Supplemental Material.

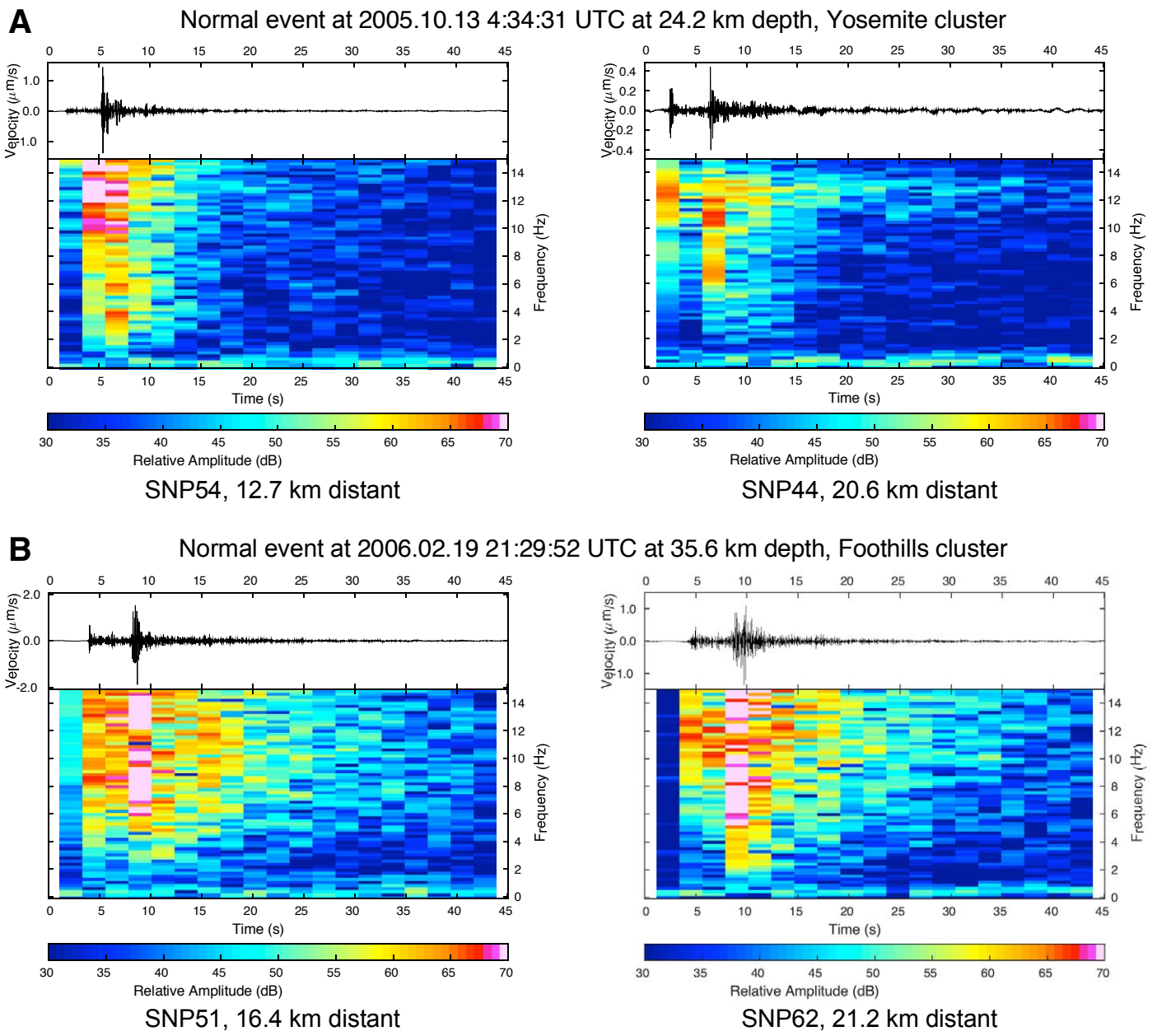

Figure 3. Vertical component seismograms and spectra for both deep normal (A and B) and long-period (C and D) earthquakes. Distances (km distant) are from the epicenter to the station. Yosemite and Foothills clusters are outlined in Figure 1 and described in the text. (*Continued on following page.*)

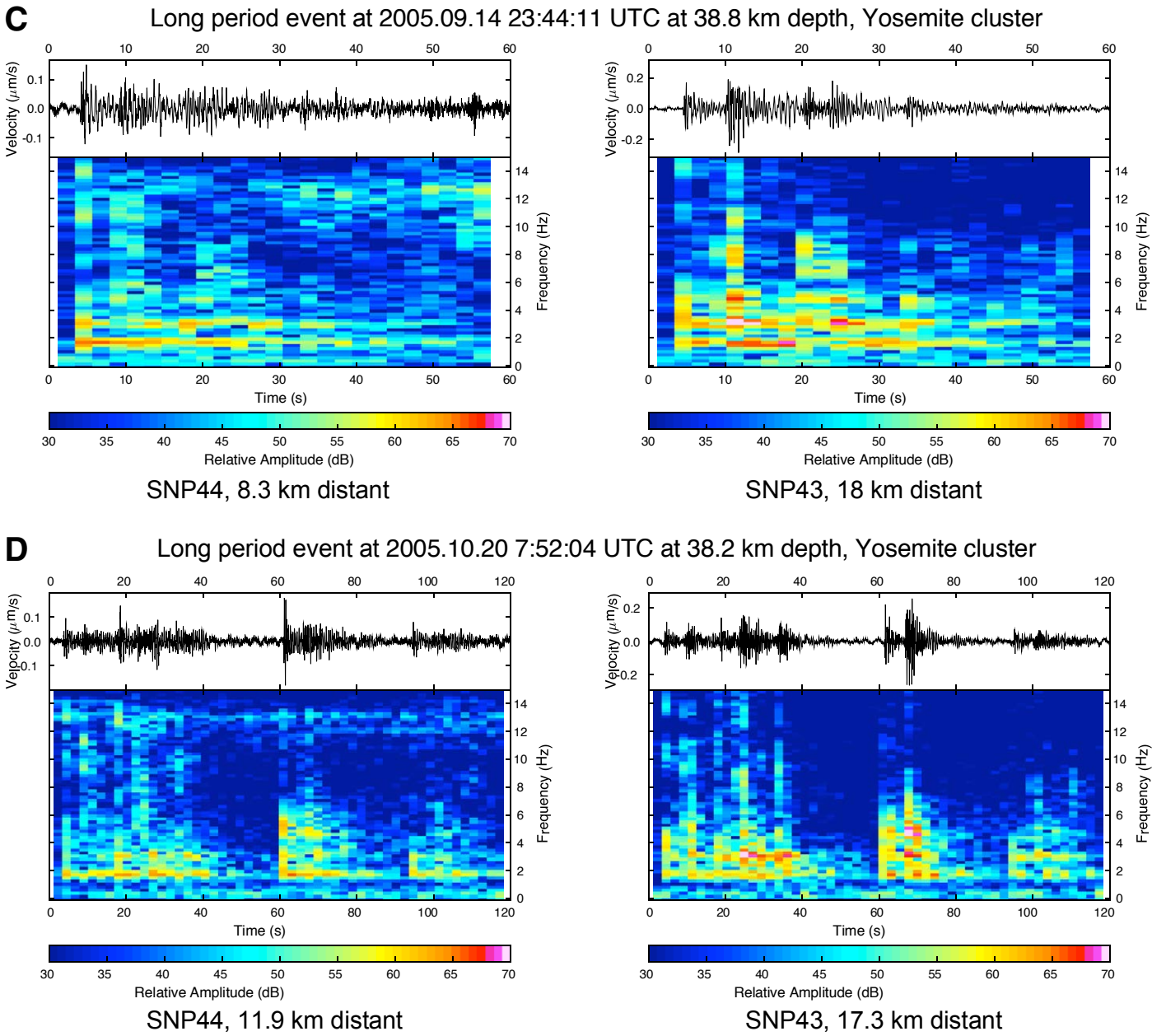

Figure 3 (*continued*).

TABLE 2. EARTHQUAKE HYPOCENTERS LOCATED WITH SIERRA NEVADA EARTHSCOPE PROJECT SEISMOMETERS

Origin time (UTC)	Latitude (°N)	Longitude (°W)	Depth (km)	Number of picks	RMS	Error (km)			Note
						Latitude	Longitude	Depth	
2005/06/11, 03:51:22.1	37.316	119.964	23.8	10	0.4	3.1	5.7	6.3	
2005/06/17, 13:27:17.7	37.437	119.731	27.8	15	0.3	2.4	4.0	4.0	
2005/06/18, 12:15:18.1	37.310	119.654	30.9	14	0.2	1.5	2.3	2.2	
2005/06/23, 15:59:28.1	37.367	119.849	29.0	17	0.3	0.9	2.2	2.4	
2005/06/24, 02:28:44.2	37.451	119.892	30.4	22	0.3	1.0	1.7	2.3	RS-1
2005/06/25, 06:15:07.0	37.196	119.738	26.0	19	0.3	1.6	2.3	2.9	
2005/06/28, 11:22:08.3	37.645	119.415	24.5	25	0.3	1.2	1.7	4.6	
2005/06/30, 07:22:52.9	37.450	119.909	30.3	30	0.5	2.0	2.8	3.9	
2005/07/05, 13:25:57.4	37.177	119.745	25.3	42	0.4	1.7	2.2	2.6	RS-2
2005/07/06, 01:50:52.5	37.198	119.736	28.1	6	0.2	3.1	3.2	3.7	RS-2
2005/07/06, 17:11:17.8	37.179	119.933	31.2	19	0.3	2.2	2.4	3.9	RS-3
2005/07/06, 23:42:22.6	37.182	119.737	27.5	16	0.3	2.4	2.5	4.2	
2005/07/16, 08:34:19.3	37.195	119.793	28.1	25	0.4	1.1	1.8	2.3	RS-4 (poor)
2005/07/20, 00:55:56.5	37.336	119.978	23.4	19	0.3	1.0	2.2	2.4	
2005/07/20, 13:32:35.9	37.190	119.925	32.7	34	0.4	1.1	1.7	2.1	RS-3
2005/07/21, 02:23:38.0	37.244	119.895	36.8	13	0.2	2.2	2.1	2.7	
2005/07/22, 08:35:53.9	37.278	119.384	33.5	33	0.3	1.5	2.3	2.9	RS-5 (mod.)
2005/07/24, 07:35:17.2	37.295	119.843	24.6	24	0.4	1.9	2.7	3.1	
2005/07/26, 09:45:35.2	37.751	120.370	19.1	25	0.4	1.5	3.7	4.3	
2005/08/04, 05:12:22.5	36.992	119.647	31.8	59	0.4	1.9	1.8	2.9	
2005/08/04, 10:04:56.1	37.489	119.832	32.5	41	0.4	1.1	1.4	2.4	
2005/08/06, 07:26:36.7	37.491	119.834	28.1	14	0.3	0.8	1.7	3.0	Group 1
2005/08/07, 04:25:18.4	36.879	119.310	28.8	14	0.2	1.5	3.1	2.9	Group 5
2005/08/07, 08:27:20.1	37.326	119.979	24.3	53	0.5	1.3	1.6	1.8	
2005/08/08, 04:54:57.8	37.187	119.739	28.0	21	0.3	2.0	2.6	3.6	
2005/08/08, 05:47:44.6	37.497	119.810	30.3	22	0.3	1.7	3.1	3.6	Group 1
2005/08/09, 22:32:49.3	37.314	119.959	25.5	14	0.4	2.5	4.0	4.3	
2005/08/12, 01:46:42.5	37.628	119.405	11.6	30	0.3	0.9	1.1	1.2	
2005/08/13, 11:51:46.0	37.496	119.803	31.0	14	0.3	2.3	4.3	3.6	Group 1
2005/08/14, 07:46:29.9	37.132	119.796	28.8	68	0.4	1.6	1.7	2.5	RS-6
2005/08/15, 02:40:57.2	37.499	119.811	31.3	16	0.3	2.3	3.7	3.2	Group 1
2005/08/21, 15:16:48.0	37.625	119.378	18.8	36	0.3	0.9	0.9	1.4	RS-7 (poor)
2005/08/22, 02:26:58.5	37.672	119.389	21.2	27	0.3	1.2	1.5	3.9	
2005/08/22, 04:12:48.7	37.084	119.894	27.9	26	0.5	2.9	4.1	4.6	
2005/08/27, 02:07:49.3	37.135	119.799	29.6	59	0.4	1.7	2.0	2.4	RS-6
2005/08/31, 04:27:08.4	36.747	119.320	22.6	8	0.0	1.3	1.2	2.0	
2005/09/03, 12:14:01.2	37.194	119.778	27.3	9	0.3	3.6	6.1	6.5	
2005/09/03, 18:23:08.6	36.882	119.305	28.1	12	0.2	1.5	3.5	3.2	Group 5
2005/09/05, 02:26:46.3	37.232	119.527	38.2	32	0.3	0.8	1.2	1.8	
2005/09/06, 12:28:03.9	36.892	119.294	28.6	16	0.2	1.7	2.4	3.1	Group 5
2005/09/11, 17:27:40.8	37.189	119.775	27.8	19	0.3	1.8	2.4	3.6	RS-4 (poor)
2005/09/14, 23:44:08.0	37.540	119.359	38.8	8	0.1	2.4	1.5	4.5	LP event
2005/09/15, 13:31:55.1	37.199	119.777	29.6	48	0.4	1.4	2.0	2.5	RS-4 (poor)
2005/09/20, 06:15:45.2	37.625	119.373	16.9	20	0.2	0.7	1.1	1.3	RS-7 (poor)
2005/09/25, 11:30:50.3	37.154	120.370	37.1	26	0.5	3.2	4.0	5.5	
2005/09/26, 05:30:46.0	37.280	119.385	32.3	62	0.3	0.9	1.0	1.1	RS-5 (mod.)
2005/09/28, 00:48:00.6	37.636	119.430	5.8	11	0.1	0.3	0.7	1.3	
2005/10/03, 04:49:45.6	37.624	119.413	10.5	5	0.1	0.5	0.9	0.0	
2005/10/03, 05:13:30.2	37.681	119.320	3.1	8	0.1	3.1	3.8	4.6	Group 4
2005/10/03, 05:15:47.8	37.679	119.318	3.1	6	0.1	3.1	3.6	4.2	
2005/10/03, 06:38:19.0	37.625	119.403	12.3	9	0.3	2.1	4.4	5.0	Group 4
2005/10/05, 07:21:34.3	37.630	119.367	15.7	13	0.2	0.5	1.3	1.4	

(*continued*)

TABLE 2. EARTHQUAKE HYPOCENTERS LOCATED WITH SIERRA NEVADA EARTHSCOPE PROJECT SEISMOMETERS (*continued*)

Origin time (UTC)	Latitude (°N)	Longitude (°W)	Depth (km)	Number of picks	RMS	Error (km)			Note
						Latitude	Longitude	Depth	
2005/10/05, 21:08:36.8	37.638	119.423	24.0	16	0.2	0.5	0.9	1.6	
2005/10/06, 01:56:47.1	37.675	119.385	21.3	19	0.2	0.6	1.3	1.4	RS-8 (mod.)
2005/10/13, 04:34:27.5	37.643	119.428	24.2	23	0.2	0.5	0.9	1.1	
2005/10/18, 01:37:39.0	36.977	119.679	19.4	21	0.3	2.0	2.4	3.6	
2005/10/18, 12:28:18.0	37.676	119.389	23.1	50	0.3	0.8	1.4	2.2	RS-8 (mod.)
2005/10/19, 23:23:59.0	37.491	119.820	32.1	36	0.4	1.1	1.5	2.1	Group 1
2005/10/20, 07:52:57.9	37.552	119.397	38.2	17	0.1	0.4	1.0	1.6	LP event
2005/10/24, 11:29:49.7	37.498	119.363	14.5	24	0.3	0.8	1.2	1.3	
2005/10/25, 08:50:53.2	36.686	119.904	18.4	18	0.3	3.3	3.0	8.8	
2005/10/28, 05:04:50.1	37.661	119.322	17.7	44	0.4	1.0	1.0	1.4	
2005/10/28, 16:48:48.4	37.322	119.993	27.1	33	0.4	1.1	1.6	2.8	
2005/11/02, 00:09:02.1	37.017	119.657	25.9	9	0.1	1.6	2.0	4.5	
2005/11/04, 14:48:32.1	37.672	119.388	21.6	26	0.2	0.6	0.9	1.2	
2005/11/05, 12:19:37.3	37.498	119.369	14.6	24	0.3	0.8	1.3	1.4	
2005/11/08, 22:06:07.2	37.531	119.406	17.5	35	0.4	1.0	1.1	1.6	
2005/11/10, 15:14:44.7	37.351	120.047	25.0	8	0.1	1.3	2.4	2.7	
2005/11/12, 19:39:30.3	37.282	119.384	32.1	78	0.3	0.9	0.8	1.1	
2005/11/19, 07:42:35.6	37.470	119.895	29.7	43	0.4	1.2	2.3	2.5	RS-1
2005/11/23, 05:22:09.3	37.014	119.650	28.3	16	0.3	2.2	2.7	5.1	RS-9 (mod.)
2005/11/25, 14:20:49.8	37.633	119.359	23.2	38	0.3	0.9	1.2	1.7	RS-10 (mod.)
2005/11/29, 01:34:32.6	37.630	119.399	13.2	23	0.2	0.7	0.9	1.3	Group 4
2005/11/29, 10:28:36.7	37.566	119.399	11.8	18	0.3	1.2	1.9	4.1	
2005/12/02, 12:13:04.8	37.631	119.367	23.9	43	0.3	0.9	0.8	1.7	
2005/12/03, 01:50:19.9	37.428	119.717	27.4	41	0.3	0.9	1.0	1.7	
2005/12/10, 04:52:12.1	37.346	119.905	34.0	37	0.3	0.9	1.2	2.2	
2005/12/17, 07:22:20.7	37.628	119.357	23.0	47	0.3	0.9	0.8	1.5	RS-10 (mod.)
2005/12/21, 17:23:21.1	37.009	119.650	29.0	20	0.3	1.9	2.5	3.6	RS-9 (mod.)
2005/12/25, 02:28:32.0	37.189	119.740	27.4	13	0.3	1.7	2.6	4.0	
2005/12/25, 20:29:01.9	37.341	119.988	19.7	5	0.0	1.3	3.4	4.0	
2005/12/26, 15:13:03.0	37.495	119.822	32.0	40	0.4	1.1	1.5	2.0	Group 1
2005/12/29, 20:42:46.3	37.405	120.021	33.8	18	0.3	0.9	1.9	3.0	Group 2
2006/01/02, 09:47:33.0	37.562	119.401	13.8	46	0.4	1.1	1.1	1.4	
2006/01/02, 11:17:47.7	37.651	119.396	3.1	6	0.1	2.7	3.2	5.1	
2006/01/05, 12:26:09.3	37.668	119.351	3.1	10	0.2	1.4	2.5	2.7	
2006/01/05, 16:08:18.9	36.872	119.284	24.5	11	0.2	1.8	2.8	3.6	
2006/01/05, 20:30:25.7	37.235	119.459	43.8	20	0.2	1.4	1.9	2.8	
2006/01/11, 12:28:36.8	37.403	120.045	28.6	5	0.0	1.9	3.9	4.7	
2006/01/11, 13:51:29.5	37.630	119.369	21.1	29	0.3	1.0	1.3	2.0	
2006/01/21, 14:12:46.4	37.405	120.036	35.0	28	0.4	1.1	1.8	2.9	
2006/01/23, 02:26:49.8	37.636	119.365	20.4	38	0.3	1.0	1.0	1.6	Group 3
2006/01/23, 02:36:01.5	37.640	119.372	19.9	23	0.2	0.9	1.6	2.5	Group 3
2006/01/23, 11:38:44.4	37.642	119.377	19.3	14	0.2	1.4	1.8	2.4	Group 3
2006/01/23, 20:24:31.5	36.690	119.278	26.1	31	0.3	2.6	1.8	2.4	
2006/01/24, 14:04:39.0	37.407	120.017	34.6	18	0.3	1.7	3.4	3.6	Group 2
2006/01/25, 11:28:58.7	37.394	120.016	34.1	21	0.3	0.9	1.8	2.9	Group 2
2006/02/03, 20:31:26.8	37.629	119.369	18.8	27	0.3	1.2	1.9	3.2	
2006/02/04, 08:07:28.1	37.145	119.826	29.2	54	0.5	1.5	1.9	3.0	
2006/02/06, 15:05:44.4	37.072	119.790	31.9	43	0.4	1.9	2.3	3.7	
2006/02/07, 13:26:29.7	37.594	119.415	8.8	57	0.4	1.1	0.9	1.3	
2006/02/12, 13:49:17.0	37.627	119.358	22.7	26	0.3	1.3	2.3	2.7	
2006/02/12, 16:27:19.8	37.421	119.366	33.4	32	0.3	0.7	1.0	1.5	
2006/02/19, 21:29:48.9	37.399	120.034	35.6	24	0.4	1.2	2.2	3.0	Group 2

(*continued*)

TABLE 2. EARTHQUAKE HYPOCENTERS LOCATED WITH SIERRA NEVADA EARTHSCOPE PROJECT SEISMOMETERS (*continued*)

Origin time (UTC)	Latitude (°N)	Longitude (°W)	Depth (km)	Number of picks	RMS	Error (km)			Note
						Latitude	Longitude	Depth	
2006/02/28, 16:20:42.6	37.208	119.455	47.4	27	0.4	1.0	1.7	2.7	
2006/03/03, 16:51:56.5	36.682	119.274	27.2	22	0.3	3.3	2.6	3.2	
2006/03/08, 10:51:50.9	37.624	119.388	16.8	22	0.3	1.1	1.9	3.3	
2006/03/10, 06:47:48.3	37.651	119.428	23.9	32	0.3	0.8	1.0	1.7	
2006/03/11, 02:33:18.3	37.693	119.420	25.2	31	0.2	0.8	1.5	1.9	
2006/03/17, 05:42:42.1	37.200	119.837	33.3	10	0.3	3.1	4.7	4.6	
2006/03/21, 11:14:31.0	37.721	119.415	27.7	44	0.3	0.8	1.0	1.1	
2006/03/21, 15:22:18.6	37.736	119.436	25.1	13	0.1	0.9	1.3	1.6	
2006/03/29, 14:21:04.3	37.275	119.579	13.1	20	0.4	1.0	1.5	2.4	
2006/04/01, 01:18:13.1	37.317	119.975	26.2	28	0.4	1.2	1.9	2.6	
2006/04/01, 01:47:21.7	37.396	120.023	34.8	25	0.3	1.0	1.5	2.7	Group 2
2006/04/06, 02:33:25.2	37.319	119.972	26.0	31	0.4	1.1	1.5	2.4	
2006/04/06, 11:02:10.9	37.640	119.404	12.6	16	0.2	0.7	1.2	1.5	
2006/04/06, 15:46:55.0	37.639	119.400	13.3	16	0.2	1.1	2.0	3.3	
2006/04/11, 12:29:01.6	37.631	119.444	3.1	22	0.4	2.3	1.3	5.3	
2006/04/14, 16:22:27.8	37.015	119.663	26.7	16	0.4	4.0	2.7	4.9	
2006/04/16, 21:28:39.0	37.187	119.735	28.0	26	0.4	1.8	2.3	4.2	
2006/04/22, 14:23:58.0	37.635	119.365	20.4	48	0.3	0.9	1.0	1.1	Group 3
2006/04/22, 18:04:12.1	37.640	119.368	19.2	22	0.3	1.1	1.8	2.8	Group 3
2006/04/23, 03:50:44.1	37.634	119.374	19.7	30	0.3	0.8	1.0	1.4	Group 3
2006/04/30, 00:33:58.3	37.628	119.378	18.4	27	0.3	1.2	2.0	3.1	Group 3
2006/05/02, 19:24:18.8	37.631	119.431	10.0	36	0.4	1.2	1.3	1.8	
2006/05/03, 08:58:26.6	37.426	119.727	27.0	34	0.4	1.1	1.5	2.1	
2006/05/03, 12:18:23.2	37.432	119.727	27.1	14	0.3	1.9	2.6	3.2	
2006/05/06, 13:00:53.1	37.409	119.748	24.9	14	0.3	0.9	1.8	2.7	
2006/05/06, 16:30:11.4	37.337	120.011	20.7	6	0.1	1.4	3.4	2.8	
2006/05/08, 04:09:13.2	37.402	119.744	24.6	26	0.4	1.1	1.5	2.9	

Note: "LP" designates the two long-period events relocated here. RS-x designations indicate repeating sets of earthquakes, with the similarity of waveforms indicated as good (no note), moderate (mod.), and poor. Larger sets of repeating earthquakes designated as groups. RMS—root mean square of travel time residuals. Error estimates represent 1σ uncertainties as determined by the HYPOCENTER program.

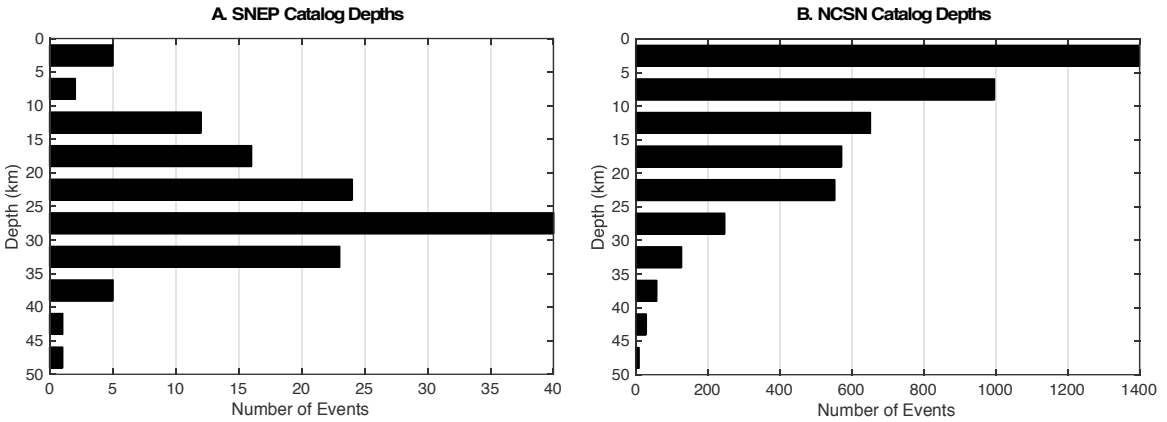

Figure 4. Depth distribution from seismic catalogs for the Sierra Nevada EarthScope Project (SNEP) (A) and the Northern California Seismic Network (NCSN) (B). More than half of the NCSN events are located in the upper 10 km, compared to <6% of those in the SNEP catalog.

were distributed over a wide range of depths with an average of 16.7 km. Earthquakes outside of either cluster are mostly scattered in the foothills and mostly occur below 20 km depth.

We can compare this event compilation with the NCSN catalog, which has 4845 earthquakes in this region (119.2°–120.5°W and 36.6°–37.8°N) from 1 January 1980 to 31 January 2017. This catalog includes 85 events during the time period of this study, 57 of which passed our detection criteria and were relocated. In addition, we identified 72 events that were not contained in the NCSN catalog for this time period. The NCSN catalog assigns magnitudes, which range from 1.21 to 2.65 (average 1.94) for events also located by the SNEP. The epicenters for these events match well, with the mean horizontal difference being 4.1 km (median of 1.9 km, minimum of 0.1 km, and maximum of 33.2 km). However, most NCSN depth estimates are considerably shallower than those determined here. Overall, events located in this study using SNEP stations are anywhere from 0.04 to 44.2 km deeper (mean of 10.7 km, median of 7.5 km) than in the NCSN catalog. The shallower event depths in the NCSN catalog compared with this study (Fig. 4B) probably result from the sparser and more asymmetrical coverage of NCSN stations and the use in the construction of the NCSN catalog of a different model of crustal wavespeed that includes a shallower (36 km) Moho than used here (Fig. 2; Oppenheimer et al., 1993; Waldhauser and Schaff, 2008).

In addition, we examine how the locations for the LP events changed. The NCSN detected 171 LP events from 1980 to 2005, most near the Yosemite cluster. Over 80% occurred between 1999 and 2002. In addition, 109 of the 168 events that predated the SNEP were located within 15 km of the LP events analyzed in this study. The other 59 LP events away from the main locus of LPs may be mislocated or mischaracterized. Until the early 2000s, most events were identified only by a handful of stations, yielding hypocenters that were anywhere from above sea level to nearly 38 km deep. For the two LP earthquakes that we reanalyzed, the NCSN originally located these events using 15–25 stations, with coverage weighted heavily toward ~22 short period stations from the NCSN that were sited in and around Mammoth Lakes. These events were originally placed at 37.8 and 36.3 km depth. Relocating with SNEP stations and a new model for crustal wavespeed resulted in minor changes to both hypocenters. Both hypocenters only deepened by 1.1–1.9 km and shifted laterally by 1.2–6.3 km. As such, the modern coverage of monitoring networks postdating the SNEP deployment may provide reasonably accurate locations of LP events in this region.

Previous studies (Wong and Savage, 1983; Miller and Mooney, 1994) noted the concentration of deep earthquakes in the area of the Foothills cluster but found comparatively few around the Yosemite cluster. This may have resulted from poor station coverage in the High Sierra. Both studies determined that seismicity in the foothills occurs less frequently outside of the main Foothills cluster. These studies also expressed uncertainty regarding the geographic extent of the lower-crustal earthquakes. The NCSN catalog displays both clusters, but also includes many events scattered outside of the clusters (Fig. 1).

We made a concerted effort to not overlook any events that met our minimum criteria throughout the western portion of the SNEP footprint. We located a handful of events east of the Foothills cluster and south of the Yosemite cluster. In addition, we also observed a few events north and west of the main zones of seismicity. Overall, the SNEP failed to detect 28 events captured by the NCSN during this period (Fig. 1), half of which occurred when the network was still being installed. These events appear in both clusters and are scattered within the San Joaquin Valley beyond the western edge of the SNEP footprint, where detections are difficult using our criteria. The aperture of the SNEP and general agreement with the distribution of seismicity seen by the NCSN suggests that few appreciable events were missed.

The statistical uncertainty in earthquakes' epicenters and depths are reported in Table 2; on average, event 1σ epicenter errors are estimated to be 2.6 km and depth errors 2.8 km. Such error estimates ignore uncertainty in the wavespeed structure. With depths largely constrained by upgoing rays to nearby stations, to first order the depth would increase directly in proportion to any underestimate in Vp. From the scatter in the VELEST models (Fig. 2; Table 3), it is plausible that our preferred model is as much as 0.1 km/s slow, which would mean our depths would be ~2%–6% too shallow, which is smaller than the uncertainties reported in Table 2. The poorer constraints on velocities below our deepest earthquakes (shaded area, Fig. 2) affects Pn (*P*-wave refraction from the top of the mantle) arrival times at distant stations, which are down-weighted and have little impact on our earthquake depths.

"Repeating" Earthquakes

Repeating earthquakes identified in this study occurred within small subgroups of events, over a broad vertical and lateral zone. The time separation of the repeating events ranges from hours to months with no discernible temporal pattern (Table 2). The vertical waveforms for these events are commonly nearly identical (Fig. 5), but similarities also appear when waveforms are rotated into the radial and tangential components. Sets of repeating earthquakes typically contain two or three events with similar waveforms. Events occurring very close in space or time may look identical, while other similarly coincident event pairs share no comparable characteristics. The Foothills cluster contains two sets of repeating earthquakes, while the Yosemite cluster contains four sets. The presence of these events suggests that future analysis of the region might benefit from the application of some style of match filter (e.g., Gibbons and Ringdal, 2006) or subspace detector approach (e.g., Harris, 2006).

Focal Mechanisms

To better understand the stress state in the crust, we examined focal mechanisms for the events in this region. We extracted 341 events from the NCSN catalog with uniquely determined focal mechanism solutions, which exhibit a full range of faulting styles (Fig. 6A). Using the classification scheme of Zoback (1992), 36% are normal or oblique normal, 25% are reverse or oblique

reverse, and 14% are strike-slip. The remaining 25% are null, which represent either extremely low-angle or extremely high-angle faulting. Wong and Savage (1983) previously found seven fault-plane solutions around the Foothills cluster but none near the Yosemite cluster. They found three strike-slip, three oblique-reverse or reverse, and one oblique-normal. Fault plane solutions from the Foothills cluster are generally consistent with a north-northeast–striking greatest principle horizontal stress direction, roughly between trends found in the San Andreas fault and Walker Lane areas (Bellier and Zoback, 1995; Zoback and Zoback, 1980; Heidbach et al., 2016; Shelly et al., 2016). The events near southern Yosemite National Park and the High Sierra hint at normal faulting typical of the Basin and Range, but predominantly exhibit a myriad of mechanisms more consistent with a heterogeneous stress state. Additional work would be needed to see if these mechanisms also reflect non-double-couple behavior such as that seen around the active Long Valley caldera just to the east (Foulger et al., 2004).

For determining first motions from SNEP seismograms, we used bandpass filters (1–5 Hz, 5–10 Hz, and 10–15 Hz with custom filters used as needed) to determine the polarity of the P-wave arrival; this is mainly to remove ambiguity introduced by the finite impulse response (FIR) filters used in recording the data. Horizontal components were rotated into radial and tangential orientations in order to best identify these arrivals. We omitted any noisy station-event pairs that did not provide definitive picks. Polarity picking was done using the MULTPLT (trace plotting, phase picking, and spectral analysis) portion of the SEISAN seismic software package (Havskov and Ottemöller, 1999; Ottemöller et al., 2017) on the first clear arrival to avoid any potential signal aliasing from

TABLE 3. WAVESPEED MODELS DEVELOPED FROM ONE-DIMENSIONAL MODELING

Vp (km/s)	Layer top depth (km)	Resolution (diagonals)	Standard deviation (km/s)
Preferred model			
5.867	0	0.872	0.301
5.979	7	0.869	0.272
6.029	10	0.862	0.284
6.137	15	0.837	0.317
6.326	20	0.861	0.290
6.431	24	0.717	0.400
6.576	27	0.856	0.295
6.577	32	0.240	0.344
7.56	47	0.000	0.000
Other models			
5.951	0	0.935	0.210
6.025	7	0.743	0.379
6.07	10	0.816	0.326
6.227	15	0.884	0.267
6.342	20	0.783	0.351
6.507	24	0.785	0.364
6.653	27	0.846	0.304
6.654	32	0.216	0.333
7.47	47	0.000	0.000
5.988	0	0.939	0.206
5.989	4	0.612	0.399
6.074	9	0.797	0.319
6.18	14	0.848	0.311
6.336	19	0.842	0.304
6.51	24	0.848	0.308
6.721	29	0.794	0.351
6.722	34	0.073	0.216
7.069	39	0.015	0.085
7.409	44	0.000	0.012
7.59	47	0.000	0.000
5.949	0	0.860	0.324
5.993	4	0.903	0.251
6.028	9	0.770	0.359
6.182	14	0.888	0.265

(*continued*)

TABLE 3. WAVESPEED MODELS DEVELOPED FROM ONE-DIMENSIONAL MODELING (*continued*)

Vp (km/s)	Layer top depth (km)	Resolution (diagonals)	Standard deviation (km/s)
6.299	19	0.806	0.330
6.499	24	0.869	0.288
6.677	29	0.775	0.363
6.678	34	0.081	0.226
7.036	39	0.014	0.084
7.389	44	0.001	0.018
7.59	47	0.000	0.000
5.929	0	0.296	0.425
6.022	2	0.936	0.207
6.027	4	0.573	0.413
6.111	8	0.883	0.253
6.271	15	0.869	0.270
6.383	21	0.797	0.341
6.646	27	0.847	0.298
6.647	32	0.156	0.298
6.823	37	0.011	0.078
7.109	42	0.005	0.054
7.52	47	0.000	0.000
5.914	0	0.266	0.397
5.997	2	0.936	0.205
6.003	4	0.538	0.399
6.007	7	0.406	0.370
6.16	11	0.900	0.249
6.214	15	0.706	0.376
6.3	19	0.741	0.363
6.504	24	0.855	0.301
6.672	29	0.744	0.386
6.677	34	0.093	0.231
7.309	44	0.002	0.031
7.43	47	0.000	0.000
Miller and Mooney (1994)			
5.24	0	0.906	
6.31	4	0.900	
6.66	12	0.906	
6.8	18	0.922	
7.98	32	0.411	

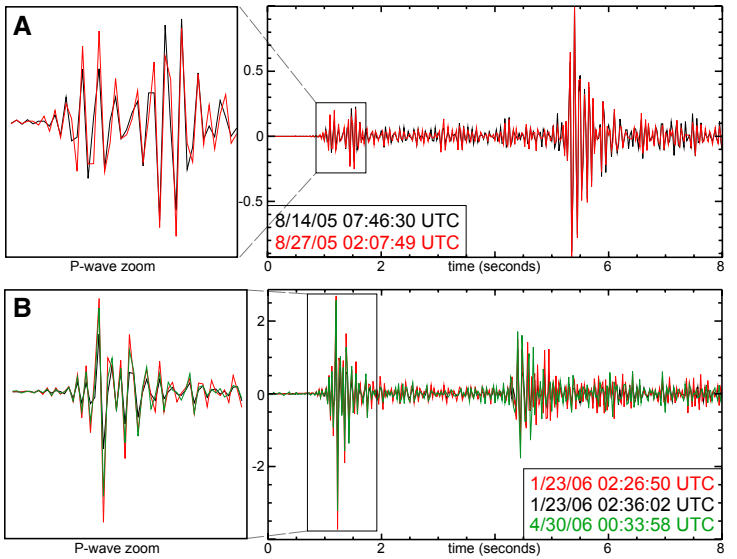

Figure 5. Examples of "repeating" earthquakes recorded by the Sierra Nevada EarthScope Project (SNEP), vertical components. (A) Two events at ~29.2 km depth within the Foothills earthquake cluster occurring 13 days apart, recorded at station SNP52. (B) Three events at ~19.6 km depth within the Yosemite earthquake cluster: two from the same day, and one more than three months later, recorded at station SNP54 (part of group 3 in Table 2). Note the S-P time of ~3–5 s, typical of most of the deeper-crustal earthquakes.

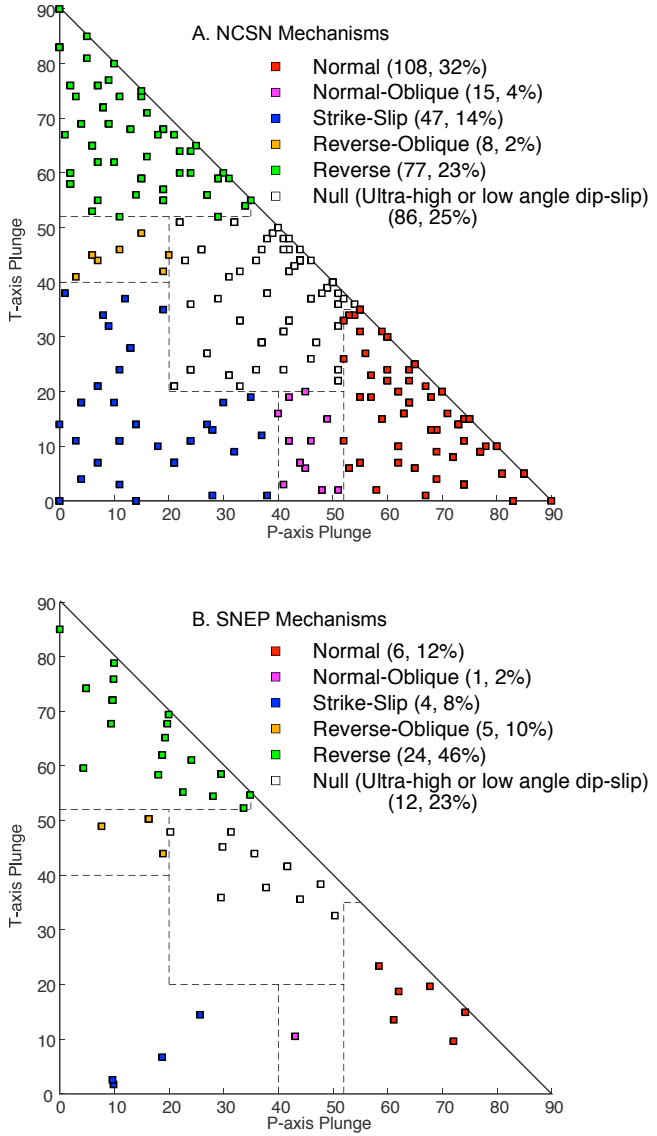

Figure 6. Fault plane solutions classified using *P*- and *T*-axis plunge for the Northern California Seismic Network (NCSN) (A) and the Sierra Nevada EarthScope Project (SNEP) (B). *P*- and *T*-axes follow usual seismological convention as the centers of the dilatational and compressional quadrants of a double-couple focal mechanism.

downsampling the data. Due to their small magnitudes, many events simply lacked a sufficient number of picks to yield a well-constrained solution.

Once calculated in FOCMEC, the fault plane solutions were graded by the similarity of solutions to one another and number of polarity errors. For each event, we investigate combinations of orientation of the seismological *P*- and *T*-axes space with a granularity of 5° on the focal sphere, i.e., not to the extent where the type of solution may change. Events with a grade of A have only solutions within 5° of one another on the focal sphere and one or fewer polarity errors. Grade B have only solutions within 5° of one another on the focal sphere and two to three polarity errors, which are typically reduced by discarding or refining a questionable pick. Grade C mechanisms may have either solutions that differ by >5° on the focal sphere, more than three polarity errors, or both; grade C mechanisms are omitted from further analysis. This resulted in 52 accepted focal mechanisms (51 grade A, one grade B) from 95 candidate events (Table 4); a subset of mechanisms spanning the range of polarity picks is shown in Figure 7.

These new focal mechanisms differ from the NCSN trends; for the SNEP, nearly half the events (47%) are characterized by reverse faulting versus 25% of NCSN mechanisms. Normal mechanisms account for only 12% and strike-slip and oblique slip mechanisms for 22% (Fig. 6B). Null mechanisms account for only 20% of the total, slightly less than the baseline from the NCSN. We find 23 fault plane solutions from the Foothills cluster, 20 from the Yosemite cluster, and nine from outside those groups (Fig. 8). The geometries of the *P*- and *T*-axes determined for these fault plane solutions vary spatially and with depth across the region (Fig. 9). *P*- and *T*-axes in the Foothills cluster tend to group well, while the mechanisms in the Yosemite cluster are more chaotic. In the Foothills cluster, *P*-axes are usually nearly north-south for both NCSN and SNEP mechanisms, while *T*-axes are steep and largely fall in an east-west band. In the Yosemite cluster, NCSN mechanisms show no organization at all, but the SNEP mechanisms tend toward near-vertical *T*-axes with shallowly plunging *P*-axes.

DISCUSSION

Crustal Deformation within the SNEP Footprint

In a regional context, the Sierra Nevada and adjacent Great Valley represent a transition between northwest-southeast–oriented right-lateral shear and northeast-southwest–oriented shortening to the west, right-lateral shear and extension in the Walker Lane bordering the eastern Sierra Nevada, and east-west–oriented extension farther east in the Basin and Range (e.g., Zoback and Zoback, 1980; Kreemer et al., 2012). The Sierra Nevada itself generally behaves as a near-rigid unit. However, localized analysis of the strain field using a reduced deformation rate tensor calculated from local seismicity (Unruh and Hauksson, 2009; Unruh et al., 2014) reveals finer-scale patterns of deformation within the Sierra Nevada. Strain in the southern Walker Lane belt appears to

TABLE 4. FAULT PLANE SOLUTIONS FOR THE 52 QUALIFYING EVENTS

Origin time (UTC)	Latitude (°N)	Longitude (°W)	Depth (km)	Strike	Dip	Rake	*P*-axis		*T*-axis		*B*-axis		# Err	Grade	No. of picks
							Trend	Plunge	Trend	Plunge	Trend	Plunge			
Foothills cluster															
2005/06/25, 06:15:07.0	37.196	119.738	26.0	104	84	–8	59	10	149	2	249	80	0	A	10
2005/07/16, 08:34:19.3	37.195	119.793	28.1	31	25	–11	16	44	242	36	133	25	0	A	13
2005/07/20, 13:32:35.9	37.190	119.925	32.7	199	25	11	167	36	34	44	277	25	0	A	18
2005/07/21, 02:23:38.0	37.244	119.895	36.8	123	61	–9	84	26	347	14	230	60	0	A	7
2005/08/06, 07:26:36.7	37.491	119.834	28.1	245	55	45	185	0	95	55	275	35	0	B	7
2005/08/07, 08:27:20.1	37.326	119.979	24.3	44	52	71	148	5	255	74	57	15	1	A	28
2005/08/08, 04:54:57.8	37.187	119.739	28.0	262	35	42	206	18	84	58	305	25	0	A	12
2005/08/08, 05:47:44.6	37.497	119.810	30.3	26	52	–27	356	43	256	11	155	45	0	A	11
2005/08/14, 07:46:29.9	37.132	119.796	28.8	238	64	44	358	8	97	49	262	40	0	A	36
2005/08/27, 02:07:49.3	37.135	119.799	29.6	235	30	0	209	38	82	38	325	30	0	A	31
2005/09/11, 17:27:40.8	37.189	119.775	27.8	275	90	70	24	42	166	42	275	20	0	A	10
2005/09/15, 13:31:55.1	37.199	119.777	29.6	138	36	73	60	10	287	76	152	10	0	A	25
2005/10/19, 23:23:59.0	37.491	119.820	32.1	2	82	–18	317	19	50	7	158	70	0	A	19
2005/10/28, 16:48:48.4	37.322	119.993	27.1	236	42	31	185	16	74	50	287	35	1	A	17
2005/11/19, 07:42:35.6	37.470	119.895	29.7	70	66	74	173	19	312	65	77	15	0	A	22
2005/12/25, 02:28:32.0	37.189	119.740	27.4	175	38	–65	189	72	67	10	334	15	0	A	8
2006/01/25, 11:28:58.7	37.394	120.016	34.1	295	81	–5	251	10	160	3	55	80	1	A	11
2006/02/04, 08:07:28.1	37.145	119.826	29.2	248	48	48	186	4	89	60	279	30	0	A	29
2006/02/06, 15:05:44.4	37.072	119.790	31.9	255	45	83	170	0	80	85	260	5	0	A	23
2006/04/01, 01:18:13.1	37.317	119.975	26.2	308	65	84	42	20	207	69	310	5	0	A	15
2006/04/01, 01:47:21.7	37.396	120.023	34.8	78	25	52	16	24	232	61	113	15	1	A	14
2006/04/16, 21:28:39.0	37.187	119.735	28.0	137	65	79	236	20	26	68	142	10	0	A	14
2006/05/03, 08:58:26.6	37.426	119.727	27.0	75	31	17	36	30	271	45	145	30	0	A	19
Yosemite cluster															
2005/06/28, 11:22:08.3	37.645	119.415	24.5	200	65	–79	131	68	282	20	15	10	0	A	13
2005/08/12, 01:46:42.5	37.628	119.405	11.6	118	71	–69	57	58	192	23	291	20	0	A	17
2005/08/21, 15:16:48.0	37.625	119.378	18.8	97	67	68	203	19	333	62	106	20	0	A	20
2005/08/22, 02:26:58.5	37.672	119.389	21.2	47	72	64	157	23	283	55	55	25	0	A	14
2005/10/03, 06:38:19.0	37.625	119.403	12.3	327	70	52	83	16	194	50	342	35	0	A	5
2005/10/05, 07:21:34.3	37.630	119.367	15.7	102	55	84	196	10	349	79	105	5	0	A	7
2005/10/06, 01:56:47.1	37.675	119.385	21.3	317	18	56	254	30	97	59	350	10	0	A	11
2005/10/13, 04:34:27.5	37.643	119.428	24.2	174	80	85	269	35	78	55	175	5	0	A	13
2005/10/18, 12:28:18.0	37.676	119.389	23.1	210	16	–18	212	48	61	38	319	15	0	A	26
2005/10/28, 05:04:50.1	37.661	119.322	17.7	26	32	–49	36	62	267	19	169	20	0	A	24
2005/11/08, 22:06:07.2	37.531	119.406	17.5	316	81	–70	248	50	29	33	132	20	0	A	18
2005/11/25, 14:20:49.8	37.633	119.359	23.2	53	42	31	2	16	251	50	104	35	0	A	18
2005/12/02, 12:13:04.8	37.631	119.367	23.9	185	75	80	283	29	81	59	188	10	0	A	22
2006/01/02, 09:47:33.0	37.562	119.401	13.8	254	90	70	3	42	145	42	254	20	0	A	24
2006/01/23, 02:26:49.8	37.636	119.365	20.4	167	57	66	273	9	27	68	180	20	0	A	19
2006/02/07, 13:26:29.7	37.594	119.415	8.8	149	25	35	100	28	322	54	201	20	0	A	33
2006/03/10, 06:47:48.3	37.651	119.428	23.9	171	67	68	277	19	47	62	180	20	0	A	17
2006/03/21, 11:14:31.0	37.721	119.415	27.7	244	32	49	184	19	54	62	281	20	0	A	22
2006/04/22, 14:23:58.0	37.635	119.365	20.4	257	56	72	0	10	122	72	267	15	0	A	24
2006/05/02, 19:24:18.8	37.631	119.431	10.0	95	80	75	198	34	347	52	98	15	0	A	20

(*continued*)

TABLE 4. FAULT PLANE SOLUTIONS FOR THE 52 QUALIFYING EVENTS (*continued*)

Origin time (UTC)	Latitude (°N)	Longitude (°W)	Depth (km)	Strike	Dip	Rake	*P*-axis		*T*-axis		*B*-axis		# Err	Grade	No. of picks
							Trend	Plunge	Trend	Plunge	Trend	Plunge			
Other events															
2005/07/22, 08:35:53.9	37.278	119.384	33.5	184	30	–80	247	74	86	15	355	5	0	A	17
2005/09/05, 02:26:46.3	37.232	119.527	38.2	345	56	72	87	10	209	72	355	15	0	A	16
2005/09/25, 11:30:50.3	37.154	120.370	37.1	75	42	67	1	5	254	74	93	15	0	A	14
2005/09/26, 05:30:46.0	37.280	119.385	32.3	28	63	–62	341	61	97	14	194	25	0	A	30
2005/11/12, 19:39:30.3	37.282	119.384	32.1	38	44	22	351	19	242	44	98	40	0	A	40
2005/12/21, 17:23:21.1	37.009	119.650	29.0	304	86	50	66	30	180	36	308	40	0	A	11
2006/02/12, 16:27:19.8	37.421	119.366	33.4	254	27	20	215	31	82	48	321	25	0	A	16
2006/02/28, 16:20:42.6	37.208	119.455	47.4	129	56	72	231	10	353	72	139	15	0	A	15
2006/03/29, 14:21:04.3	37.275	119.579	13.1	278	40	26	231	20	116	48	336	35	0	A	12

Note: Units for faulting orientation are degrees clockwise from north (strike, trend) or from horizontal (dip, rake, plunge). Dip direction is clockwise from the strike azimuth. Rake is measured upward from strike azimuth within the fault plane and represents the motion of the upper side of the fault relative to the lower side. *P*- and *T*-axes defined in Figure 6 caption. The *B*-axis is perpendicular to the other two and is parallel to the intersection of the fault and auxiliary planes. # Err—number of polarity picks violated by the preferred solution. Grade is defined in the text. No. of picks— number of polarity observations for that event.

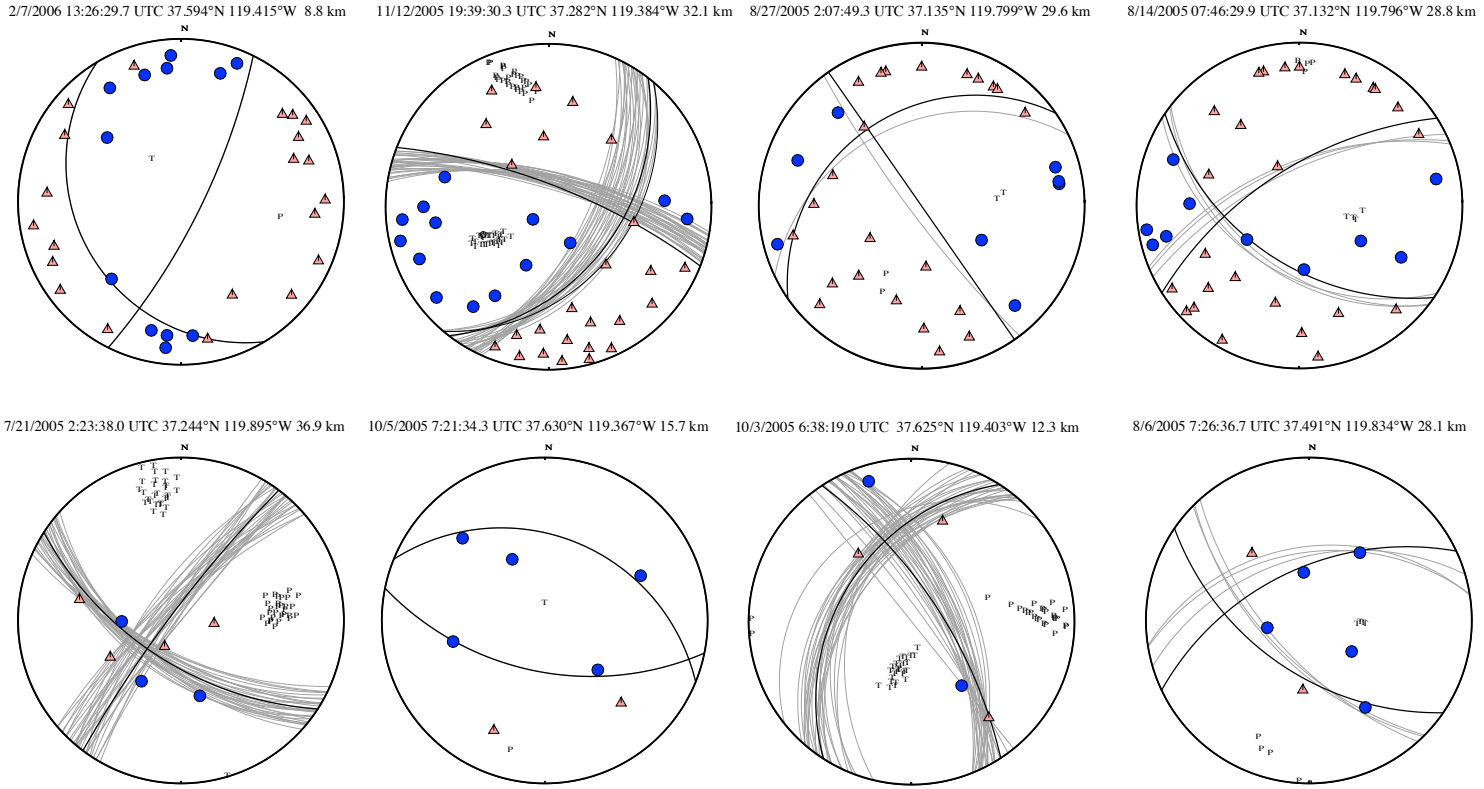

Figure 7. Eight example first-motion focal mechanisms on lower-hemisphere stereographic projections. Pink triangles are dilatational first motions; blue circles, compressional first motions. P and T characters positioned at the *P*- and *T*-axes for acceptable solutions. See Figure 6 caption for *P*- and *T*-axes definitions. Heavy black fault planes are those listed in Table 4. Numbers above each plot are the date and time of the earthquake and its latitude, longitude, and depth.

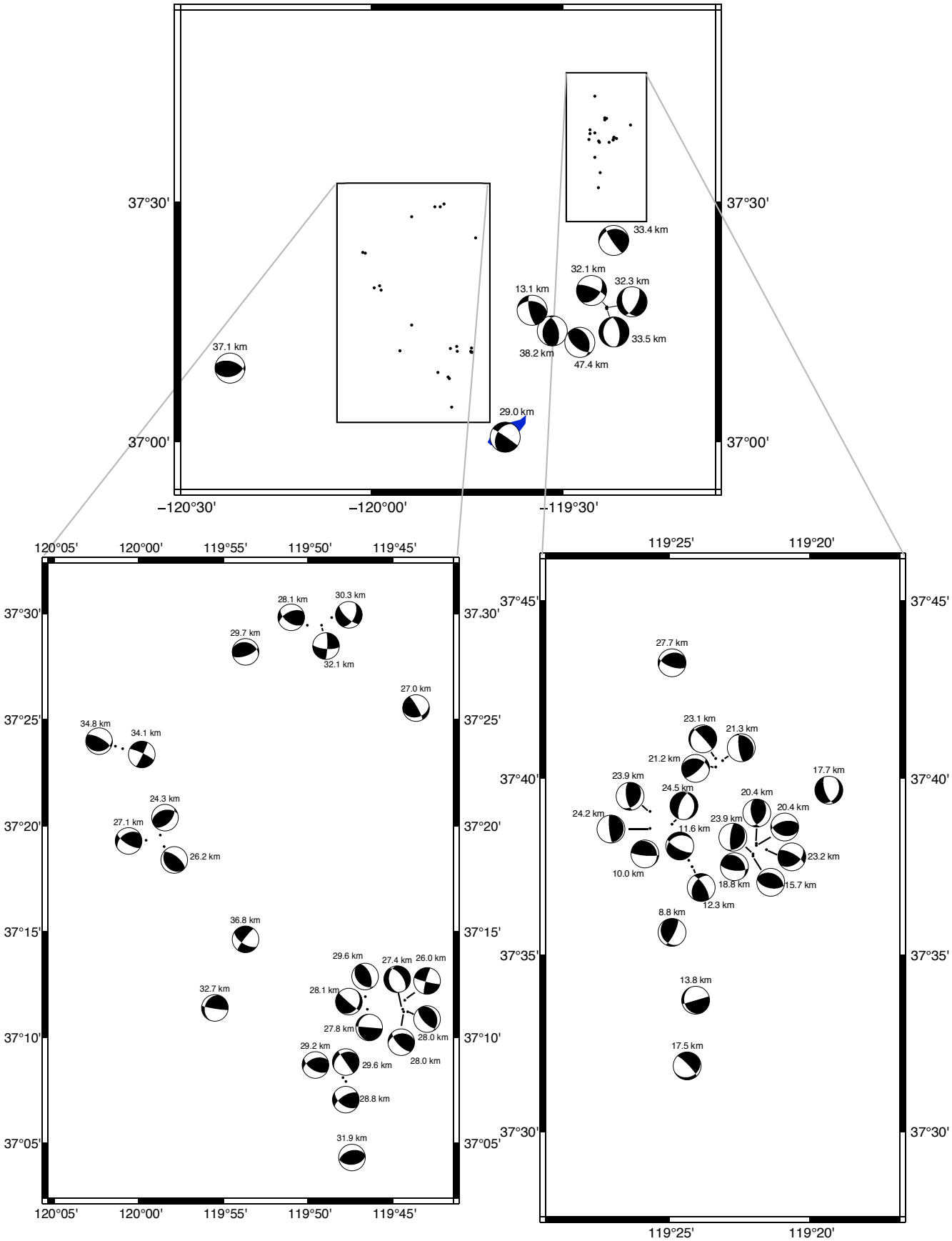

Figure 8. Lower-hemisphere plots of earthquake focal mechanisms determined with the Sierra Nevada EarthScope Project (SNEP) data set. Black sections are the compressional quadrants. Earthquake depths indicated by each focal sphere.

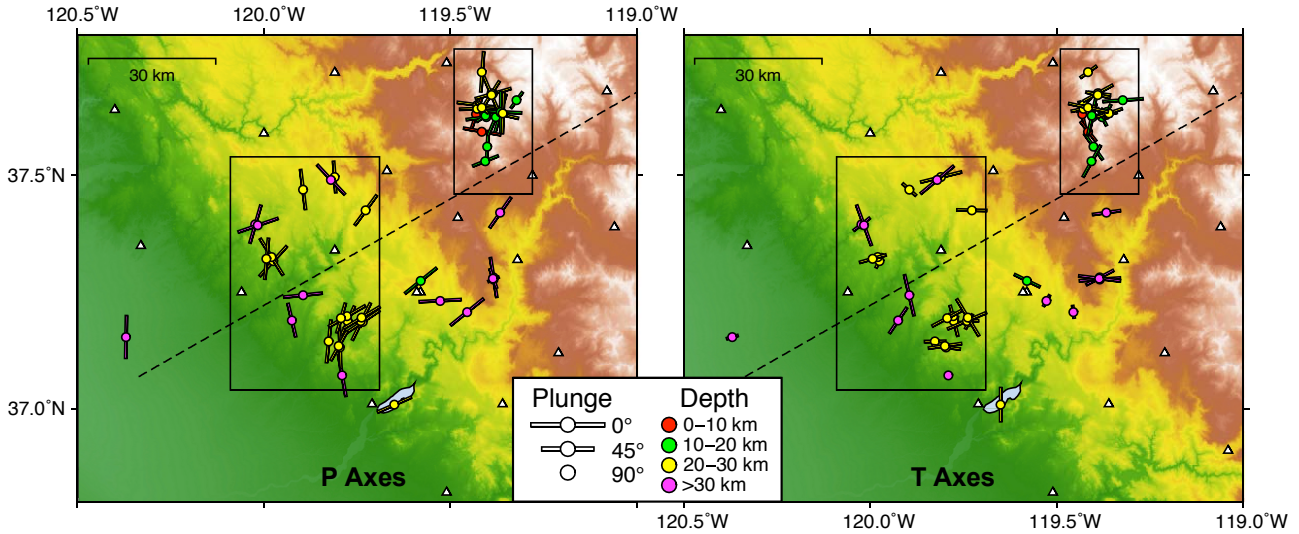

Figure 9. Map-view of trends of *P*-axes (left) and *T*-axes (right) (see Figure 6 caption for definitions of *P*- and *T*-axes), symbolized by plunge angle and colored by earthquake depth.

be simple shear, accommodating northwest translation of the Sierra Nevada block with coincident crustal thinning. However, the southeastern Sierra is shown to be elongating and flattening horizontally south of ~36.5°N and especially due east of the Isabella anomaly (Unruh et al., 2014). This is coincident with thinned crust that is observed with receiver functions above inflowing mantle asthenosphere (Frassetto et al., 2011; Jones et al., 2014). This can be interpreted as a consequence of lithosphere thickening and foundering to the west within the Isabella anomaly (Unruh and Hauksson, 2009). Unruh et al. (2014) speculated that a rotation of the strain field in this part of the Sierra Nevada foothills and adjacent San Joaquin Valley is the response of the crust to rebound in the late stages of lithospheric foundering.

The focal mechanisms calculated using the SNEP provide a better picture of the crustal strain-rate field northwest of the proposed location of foundering in the lower lithosphere. The Foothills cluster is within the Sierran Foothills wavespeed anomaly; both clusters are ~50 km from the northern edge of the Isabella anomaly as resolved in recent teleseismic P-wave tomography (Jones et al., 2014). We calculated the reduced deformation rate tensor for these events (Twiss and Unruh, 1998; Unruh and Hauksson, 2009), which yields a transpressional strain-rate field with significant components of net vertical thickening for both groups of earthquakes. Maximum shortening trends are ENE-WSW for the Yosemite cluster and NNE-SSW for the Foothills cluster, in both cases differing from the regional trends of north-south shortening for the Walker Lane and northeast-southwest for the San Andreas transform. Intriguingly, the Foothills cluster mechanisms suggest triaxial deformation, with shortening on both NNE-SSW and ENE-WSW orientations and vertical lengthening. Both groups of events would benefit from more complete, robust event data sets in order to refine these patterns.

Lithospheric Structure and Crustal Seismicity

Moderate to large teleseismic earthquakes recorded by the SNEP were used to map discontinuities within and between the crust and upper mantle with teleseismic receiver functions, which allows us to place local seismicity in structural context (Frassetto et al., 2011). We focus on one profile (Fig. 10) oriented ENE-WSW that runs just south of the events in the Yosemite cluster and bisects the Foothills cluster (Fig. 1). Events occurring 15 km north and south of this transect are projected onto it, roughly matching the lateral sensitivity and averaging of the receiver functions.

The Foothills cluster earthquakes occurred entirely between 19 and 40 km depth (average 28.9 km), overlying the region of a diffuse Moho conversion described by Frassetto et al. (2011). The events appeared in a few distinct pockets, none of which coincide with any structural features resolved by receiver functions. We did not locate a single earthquake above 19 km depth in this cluster, indicating that this seismicity might lie under a décollement. This is very similar to the depth distribution of earthquakes in this area determined by Wong and Savage (1983), which was restricted to between ~15 and 40 km depth. The persistent absence of shallow events separates this deep cluster

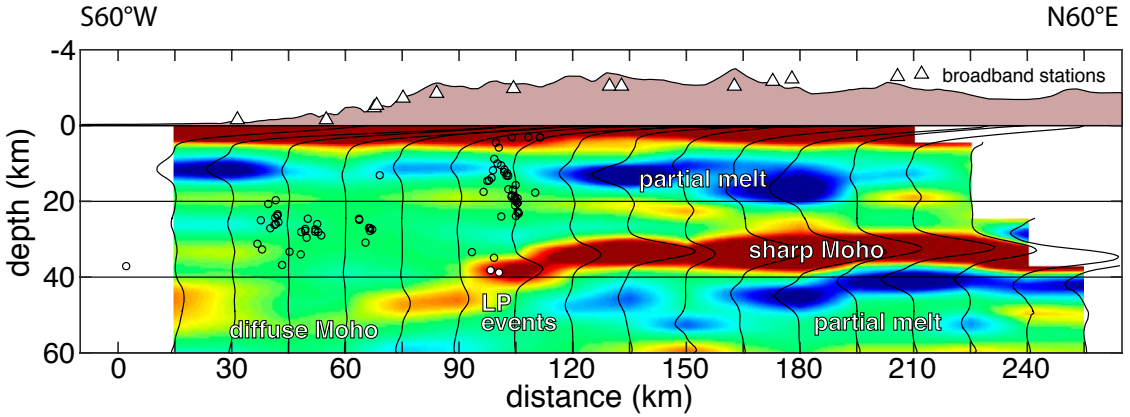

Figure 10. Receiver function profile with overlaid earthquakes from this study (circles), modified from section K-K′ of Frassetto et al. (2011) and located in Figure 1. Stations and earthquakes within 30 km on both sides of the transect are included in profile. Prominent features are labeled. LP—long-period. Positive Ps conversions are red and negative conversions are blue, each saturating out at 10% of the direct P arrival.

from other more-ephemeral deep seismicity that is then followed by shallower events (e.g., Smith et al., 2004, 2016). The absence of seismicity in the surrounding region near 20 km depth suggests that this cluster is not the deeper manifestation of shallower seismicity elsewhere, a suggestion reinforced by the different shortening directions when compared with surrounding seismicity. Thus, this seismicity might be independent of the surface tectonics.

The Yosemite cluster maps into a compact, linear trend through the crust within the Sierra Nevada batholith, ranging from 25 km depth to near the surface (average 16.7 km). The deep LP events underlie the Yosemite cluster along the Moho at 38–39 km depth, at the point separating a shallow and bright Moho receiver-function conversion to the east from the deeper and more diffuse conversion to the west. Although scattered, two-thirds of the older LP events in the NCSN catalog are located within 15 km of these events, albeit with highly varying depths. As noted before, we suspect that these older depths are questionable owing to the known challenge of constraining depth in an earthquake location from a distant network. Most of these LP events are just to the north of the two we analyzed, associating even more strongly with our observations in the Yosemite cluster.

Long-period earthquakes occur beneath several active volcanic centers in the southern Cascade Range–Sierra Nevada including Mount Shasta, Mount Lassen, and Mammoth Mountain. These earthquakes locate at depths from 10 to 35 km, and are usually found to coincide with shallower clusters of small-magnitude earthquakes. These LP events have been suggested to occur in relation to periods of magmatic migration and magmatic-hydrothermal interactions in the crust (Pitt et al., 2002). The LP earthquakes here situate at least 12 km deeper and 10 km south of the Yosemite cluster, but we cannot ascertain a direct connection between the two styles of deformation without additional observations.

Sequences of unusual lower-crustal seismicity near Lake Tahoe (Smith et al., 2004, 2016; von Seggern et al., 2008), which consisted of two dense, linear clusters of deep crustal (>20 km) earthquakes, may offer insights into the factors driving seismicity within the Yosemite cluster. The first Lake Tahoe cluster occurred beneath northwestern Lake Tahoe in 2003 and was followed by a shallower swarm active from 2003 to 2005. The second cluster happened near Sierra Valley in 2011 and was preceded by a larger deep-crustal earthquake located between the swarms. Smith et al. (2004, 2016) suggested that the deep swarm originated from a magmatic intrusion into the lower crust, and the corresponding shallow swarm is a stress-triggered response. Focal mechanisms for many of the shallower Lake Tahoe events exhibit *P*- and *T*-axes consistent with the regional stress field. However, the mechanisms for the earthquakes in the deeper cluster display scattered *P*- and *T*-axes. The distribution of events in the Yosemite cluster resembles the planar swarm of earthquakes beneath Lake Tahoe (von Seggern et al., 2008). Similar to those for the deeper Lake Tahoe events, the focal mechanisms for the Yosemite cluster are inconsistent with regional stress patterns. The similar characteristics of these clusters of seismicity may indicate that they resulted from a common mechanism.

Previous studies have not considered the role of crustal seismicity, particularly the unusually deep or LP events, when suggesting that lithospheric foundering occurs only in the southern Sierra Nevada (e.g., Zandt, 2003) or along the entire batholith (Jones et al., 2004). With the exception of reservoir-induced events, seismicity along the western Sierra Nevada and its foothills north of ~38°N is largely absent in historical records (NCEDC, 2014). The limited spatial extent of deep and LP events suggests that a geographically focused process is responsible for the earthquakes identified here. The diminished level of seismicity north of ~38°N coincides with a transition in surface geology from prominently batholithic crust to the south to primarily metamorphic rock to the north.

Several lines of evidence suggest that the Foothills cluster most likely represents some phase of lithospheric foundering. The absence of any connection to surface deformation suggests a local source of stress acting under

some kind of detachment. The different strain-rate orientation compared to other seismicity suggests a local source of stress. This seismicity is occurring in high-wavespeed and thus probably high-density lower crust, an inference compatible with the fairly high-isostatic-gravity anomalies (0 to +10 mGal) in this area (Oliver et al., 1993). Localized thickening of dense lower crust and/or uppermost mantle appears to be occurring. An alternative could be impingement of some deeper body against the base of the lithosphere (e.g., a northern extension of the proposed Monterey plate; Wang et al., 2013), but the proposed position of such a body is both well to the south and much too deep. Additionally, any impingement would presumably be stronger where the body was shallower, yet similar seismicity is absent in the surrounding areas. Finally, teleseismic tomography (Jones et al., 2014, their figure 17) and magnetotellurics (Ostos and Park, 2012) in this area suggest that some dynamic process is affecting the lithosphere near the Moho just to the east, which might also explain the LP events and the Yosemite cluster, thus possibly providing the means for the lower crust or lithospheric mantle to become gravitationally unstable.

Crustal Wavespeeds

Past investigations of crustal wavespeeds of the Sierra Nevada region found a wide range of results (Bateman and Eaton, 1967; Holbrook and Mooney, 1987; Miller and Mooney, 1994; Savage et al., 2003; Fliedner et al., 1996, 2000; Ruppert et al., 1998; Prodehl, 1979; Spieth et al., 1981). Miller and Mooney (1994) interpreted this heterogeneity to be a marker of the many different tectonic provinces and crustal compositions that characterize the area. Our model most resembles the wavespeed structure from Fliedner et al. (1996) under the western Sierra Nevada foothills to the south; we do not see the rapid increase in wavespeed in the upper crust found farther west (Fliedner et al., 2000; Miller and Mooney, 1994).

The smoother transition between layer wavespeeds in our model compared to that of Miller and Mooney (1994) may be from the slightly different regions sampled by each study. The earthquakes in the Foothills cluster likely record higher wavespeeds associated with metamorphic rocks found beneath the western foothills. In contrast, Yosemite cluster earthquakes record the intermediate wavespeeds associated with the granitic composition of the batholith itself. A vast majority of earthquakes used by Miller and Mooney (1994) were from the Foothills cluster region, and the stations recording these events were exclusively to the north in the metamorphic belt of the western Sierra Nevada. Therefore, the raypaths were nearly entirely outside the batholith, which explains why they observed much higher wavespeeds and more abrupt transitions from 4 to 12 km depth than we see in our preferred model over the same depth interval. Results from Ruppert et al. (1998) showing upper-crustal wavespeeds of 6.0–6.4 km/s and a lower-crustal wavespeed of 6.6 km/s beneath the southern Sierra Nevada batholith are much more consistent with our findings, as are results from Fliedner et al. (2000) that find wavespeeds of 5.9–6.3 km/s below the batholith. Our model loses resolution below 35 km, but forward modeling of receiver functions suggests that a gradual increase in wavespeed persists to at least 70 km depth (Frassetto et al., 2011). The lack of any sharp boundary is consistent with an arc root beneath the region that is structurally intact.

CONCLUSIONS

With the observations from the SNEP deployment, we place in a broader, geodynamic context the unusual seismicity distributed across the central High Sierra and adjacent western foothills. Small, commonly very deep crustal earthquakes in two distinct clusters show a unique and distinct tectonic process occurring within the Sierra Nevada batholith. Previous studies suggested the presence of a partially removed and actively foundering eclogitic root beneath the southern Sierra Nevada crust, and we demonstrate that the observed earthquakes are a potential seismic consequence of this. Events occurring in the Foothills cluster may be a response to stressing of the lower crust due to active root foundering. Those in the Yosemite cluster beneath the High Sierra may be related to inflow of adjacent mantle asthenosphere stressing the overlying crust or magmatic activity within the crust itself.

A one-dimensional P- wavespeed model for the south-central Sierra Nevada created by inverting crustal earthquake data suggests a very gradual wavespeed increase with depth, from ~5.8 km/s at the surface to ~6.7 km/s at ~35 km. If the presence of deep-crustal earthquake activity is an indication of active root removal, as we suggest, then the extent of removal in the southern Sierra Nevada does not extend northward of ~37.5°N. It is important to note that the seismic data used in this study spans only the central portion of the batholith, which precludes our ability to make any conclusions regarding root removal farther north or south. Existing seismic catalogs, however, can be interpreted to indicate that there appears to be no seismogenically active, large-scale root removal along the entire strike of the batholith.

ACKNOWLEDGMENTS

We thank the SNEP field teams for installing, operating, and removing the array. We are also especially grateful to the private landowners who allowed us to deploy on their land. Edi Kissling provided support for VELEST and offered comments on our initial results. PASSCAL Quick Look (PQL) and Seismic Analysis Code (SAC) were used throughout this analysis. We also thank Glenn Thompson and Jackie Caplan-Auerbach for technical assistance with GISMO and spectrogram plotting, and David Shelly and Mike Brudzinski for assistance accessing the NCSN catalog and working with the fault plane solutions. Two anonymous reviews strengthened this presentation. This work was supported by U.S. National Science Foundation (NSF) EarthScope grants EAR-0454554, EAR-0454524, and EAR-0454535 to the Universities of Arizona, Colorado, and South Carolina. The seismic instruments were provided by the Incorporated Research Institutions for Seismology (IRIS) through the PASSCAL Instrument Center at New Mexico Tech. Data from the TA network were made freely available as part of the EarthScope USArray facility, operated by IRIS. The facilities of the IRIS Data Management Center were used for access to waveforms, related metadata, and/or derived products used in this study. These facilities are supported by the NSF under Cooperative Agreement EAR-1261681 and the U.S. Department of Energy National Nuclear Security Administration.

REFERENCES CITED

Bateman, P.C., and Eaton, J.P., 1967, Sierra Nevada batholith: Science, v. 158, p. 1407–1417, https://doi.org/10.1126/science.158.3807.1407.

Bateman, P.C., and Wahrhaftig, C., 1966, Geology of the Sierra Nevada, *in* Bailey, E.H., ed., Geology of Northern California: California Division of Mines and Geology Bulletin 190, p. 107–184.

Bellier, O., and Zoback, M.L., 1995, Recent state of stress change in the Walker Lane zone, western Basin and Range province, United States: Tectonics, v. 14, p. 564–593, https://doi.org/10.1029/94TC00596.

Benz, H.M., and Zandt, G., 1993, Teleseismic tomography: Lithospheric structure of the San Andreas Fault system in northern and central California, *in* Iyer, H.M., and Hirahara, K., eds., Seismic Tomography: Theory and Practice: New York, Chapman and Hall, p. 440–465.

Biasi, G.P., and Humphreys, E.D., 1992, P-wave image of the upper mantle structure of central California and southern Nevada: Geophysical Research Letters, v. 19, p. 1161–1164, https://doi.org/10.1029/92GL00439.

Busby, C.J., and Putirka, K., 2009, Miocene evolution of the western edge of the Nevadaplano in the central and northern Sierra Nevada: Paleocanyons, magmatism, and structure: International Geology Review, v. 51, p. 670–701, https://doi.org/10.1080/00206810902978265.

Christensen, M.N., 1966, Late Cenozoic crustal movements in the Sierra Nevada of California: Geological Society of America Bulletin, v. 77, p. 163–181, https://doi.org/10.1130/0016-7606(1966)77[163:LCCMIT]2.0.CO;2.

Cousens, B., Prytulak, J., Henry, C., Alcazar, A., and Brownrigg, T., 2008, Geology, geochronology, and geochemistry of the Miocene–Pliocene Ancestral Cascades arc, northern Sierra Nevada, California and Nevada: The roles of the upper mantle, subducting slab, and the Sierra Nevada lithosphere: Geosphere, v. 4, p. 829–853, https://doi.org/10.1130/GES00166.1.

Dickinson, W.R., 1979, Cenozoic plate tectonic setting of the Cordilleran region in the United States, *in* Armentrout, J.M., Cole, M.R., and TerBest, H., eds., Cenozoic Paleogeography of the Western United States: Proceedings, Pacific Coast Paleogeography Symposium, 3rd, Los Angeles: Pacific Section, Society of Economic Paleontologists and Mineralogists, p. 1–13.

Dickinson, W.R., 2008, Accretionary Mesozoic–Cenozoic expansion of the Cordilleran continental margin in California and adjacent Oregon: Geosphere, v. 4, p. 329–353, https://doi.org/10.1130/GES00105.1.

Dodge, F.C.W., and Moore, J.G., 1981, Late Cenozoic volcanic rocks of the southern Sierra Nevada, California: II. Geochemistry: Summary: Geological Society of America Bulletin, v. 92, p. 912–914 (pt 1), 1670–1761 (pt 2), https://doi.org/10.1130/0016-7606(1981)92<912:LCVROT>2.0.CO;2.

Ducea, M.N., 2001, The California arc: Thick granitic batholiths, eclogitic residues, lithospheric-scale thrusting, and magmatic flare-ups: GSA Today, v. 11, no. 11, p. 4–10, https://doi.org/10.1130/1052-5173(2001)011<0004:TCATGB>2.0.CO;2.

Ducea, M.N., and Saleeby, J.B., 1996, Buoyancy sources for a large, unrooted mountain range, the Sierra Nevada, California: Evidence from xenolith thermobarometry: Journal of Geophysical Research, v. 101, p. 8229–8244, https://doi.org/10.1029/95JB03452.

Ducea, M.N., and Saleeby, J.B., 1998a, The age and origin of a thick mafic-ultramafic keel from beneath the Sierra Nevada batholiths: Contributions to Mineralogy and Petrology, v. 133, p. 169–185, https://doi.org/10.1007/s004100050445.

Ducea, M.N., and Saleeby, J.B., 1998b, A case for delamination of the deep batholithic crust beneath the Sierra Nevada, California: International Geology Review, v. 40, p. 78–93, https://doi.org/10.1080/00206819809465199.

Fliedner, M.M., Ruppert, S.D., Malin, P.E., Park, S.K., Jiracek, G.R., Phinney, R.A., Saleeby, J.B., Wernicke, B.P., Clayton, R.W., Keller, G.R., Miller, K.C., Jones, C.H., Luetgert, J.H., Mooney, W.D., Oliver, H.L., Klemperer, S.L., and Thompson, G.A., 1996, Three-dimensional crustal structure of the southern Sierra Nevada from seismic fan profiles and gravity modeling: Geology, v. 24, p. 367–370, https://doi.org/10.1130/0091-7613(1996)024<0367:TDCSOT>2.3.CO;2.

Fliedner, M.M., Klemperer, S.L., and Christensen, N.I., 2000, Three-dimensional seismic model of the Sierra Nevada arc, California, and its implications for crustal and upper mantle composition: Journal of Geophysical Research, v. 105, p. 10,899–10,921, https://doi.org/10.1029/2000JB900029.

Foulger, G.R., Julian, B.R., Hill, D.P., Pitt, A.M., Malin, P.E., and Shalev, E., 2004, Non-double-couple microearthquakes at Long Valley caldera, California, provide evidence for hydraulic fracturing: Journal of Volcanology and Geothermal Research, v. 132, p. 45–71, https://doi.org/10.1016/S0377-0273(03)00420-7.

Frassetto, A.M., Zandt, G., Gilbert, H., Owens, T.J., and Jones, C.H., 2011, Structure of the Sierra Nevada from receiver functions and implications for lithospheric foundering: Geosphere, v. 7, p. 898–921, https://doi.org/10.1130/GES00570.1.

Frohlich, C., Gan, W., and Herrmann, R.B., 2014, Two deep earthquakes in Wyoming: Seismological Research Letters, v. 86, p. 810–818, https://doi.org/10.1785/0220140197.

Gibbons, S.J., and Ringdal, F., 2006, The detection of low magnitude seismic events using array-based waveform correlation: Geophysical Journal International, v. 165, p. 149–166, https://doi.org/10.1111/j.1365-246X.2006.02865.x.

Gilbert, H., Yang, Y., Forsyth, D.W., Jones, C.H., Owens, T.J., Zandt, G., and Stachnik, J.C., 2012, Imaging lithospheric foundering in the structure of the Sierra Nevada: Geosphere, v. 8, p. 1310–1330, https://doi.org/10.1130/GES00790.1.

Gomberg, J.S., Shedlock, K.M., and Roecker, S.W., 1990, The effect of S-wave arrival times on the accuracy of hypocenter estimation: Bulletin of the Seismological Society of America, v. 80, p. 1605–1628.

Harris, D.B., 2006. Subspace detectors: Theory: U.S. Department of Energy Technical Report UCRL-TR-222758, https://doi.org/10.2172/900081.

Havskov, J., and Ottemöller, L., 1999, SeisAn earthquake analysis software: Seismological Research Letters, v. 70, p. 532–534, https://doi.org/10.1785/gssrl.70.5.532.

Heidbach, O., Rajabi, M., Reiter, K., Ziegler, M., and WSM Team, 2016, World Stress Map database release 2016, v. 1: Potsdam, Germany, GFZ Data Services, https://doi.org/10.5880/WSM.2016.001.

Holbrook, W.S., and Mooney, W.D., 1987, The crustal structure of the axis of the Great Valley, California, from seismic refraction measurements: Tectonophysics, v. 140, p. 49–63, https://doi.org/10.1016/0040-1951(87)90139-9.

House, M.A., Wernicke, B.P., and Farley, K.A., 1998, Dating topography of the Sierra Nevada, California, using apatite (U-Th)/He ages: Nature, v. 396, p. 66–69, https://doi.org/10.1038/23926.

Jennings, C.W., and Bryant, W.A., 2010, Fault activity map of California: California Geological Survey Geologic Data Map 6, scale 1:750,000.

Jones, C.H., Kanamori, H., and Roecker, S.W., 1994, Missing roots and mantle "drips": Regional P_n and teleseismic arrival times in the southern Sierra Nevada and vicinity, California: Journal of Geophysical Research, v. 99, p. 4567–4601, https://doi.org/10.1029/93JB01232.

Jones, C.H., Farmer, G.L., and Unruh, J., 2004, Tectonics of Pliocene removal of lithosphere of the Sierra Nevada, California: Geological Society of America Bulletin, v. 116, p. 1408–1422, https://doi.org/10.1130/B25397.1.

Jones, C.H., Reeg, H., Zandt, G., Gilbert, H., Owens, T.J., and Stachnik, J., 2014, P-wave tomography of potential convective downwellings and their source regions, Sierra Nevada, California: Geosphere, v. 10, p. 505–533, https://doi.org/10.1130/GES00961.1.

Kissling, E., Ellsworth, W.L., Eberhart-Phillips, D., and Kradolfer, U., 1994, Initial reference models in local earthquake tomography: Journal of Geophysical Research, v. 99, p. 19,635–19,646, https://doi.org/10.1029/93JB03138.

Kreemer, C., Hammond, W.C., Blewitt, G., Holland, A.A., and Bennett, R.A., 2012, A geodetic strain rate model for the Pacific–North American plate boundary, western United States: Nevada Bureau of Mines and Geology Map 178, scale 1:1,500,000.

Lee, C.-T., Rudnick, R.L., and Brimhall, G.H., Jr., 2001, Deep lithospheric dynamics beneath the Sierra Nevada during the Mesozoic and Cenozoic as inferred from xenolith petrology: Geochemistry Geophysics Geosystems, v. 2, 1053, https://doi.org/10.1029/2001GC000152.

Lienert, B.R., and Havskov, J., 1995, A computer program for locating earthquakes both locally and globally: Seismological Research Letters, v. 66, p. 26–36, https://doi.org/10.1785/gssrl.66.5.26.

Manley, C.R., Glazner, A.F., and Farmer, G.L., 2000, Timing of volcanism in the Sierra Nevada of California: Evidence for the Pliocene delamination of the batholithic root?: Geology, v. 28, p. 811–814, https://doi.org/10.1130/0091-7613(2000)28<811:TOVITS>2.0.CO;2.

Miller, K.C., and Mooney, W.D., 1994, Crustal structure and composition of the southern Foothills Metamorphic Belt, Sierra Nevada, California, from seismic data: Journal of Geophysical Research, v. 99, p. 6865–6880, https://doi.org/10.1029/93JB02755.

Moore, J.G., and Dodge, F.C.W., 1980, Late Cenozoic volcanic rocks of the southern Sierra Nevada, California: I. Geology and petrology: Summary: Geological Society of America Bulletin, v. 91, p. 515–518 (pt 1), p. 1995–2038 (pt 2), https://doi.org/10.1130/0016-7606(1980)91<515:LCVROT>2.0.CO;2.

Mulch, A., Graham, S.A., and Chamberlain, C.P., 2006, Hydrogen isotopes in Eocene river gravels and paleoelevation of the Sierra Nevada: Science, v. 313, p. 87–89, https://doi.org/10.1126/science.1125986.

NCEDC (Northern California Earthquake Data Center), 2014, Northern California Earthquake Data Center: Berkeley, California, University of California Berkeley Seismological Laboratory, https://doi.org/10.7932/NCEDC.

Oliver, H.W., Moore, J.G., and Sikora, R.F., 1993, Internal structure of the Sierra Nevada batholith based on specific gravity and gravity measurements: Geophysical Research Letters, v. 20, p. 2179–2182, https://doi.org/10.1029/93GL01379.
Oppenheimer, D., Klein, F., Eaton, J., and Lester, F., 1993, The Northern California Seismic Network bulletin, January–December 1992: U.S. Geological Survey Open-File Report 93-578, 45 p.
O'Rourke, C.T., Sheehan, A.F., Erslev, E.A., and Anderson, M.L., 2016, Small-magnitude earthquakes in north-central Wyoming recorded during the Bighorn Arch seismic experiment: Bulletin of the Seismological Society of America, v. 106, p. 281–288, https://doi.org/10.1785/0120150114.
Ostos, L., and Park, S.K., 2012, Foundering lithosphere imaged with magnetotelluric data beneath Yosemite National Park, California: Geosphere, v. 8, p. 98–104, https://doi.org/10.1130/GES00657.1.
Ottemöller, L., Voss, P., and Havskov, J., 2017, SEISAN earthquake analysis software for Windows, Solaris, Linux and MacOSx, v. 10.5: http://seis.geus.net/software/seisan/seisan.html.
Owens, T., Jones, C., and Zandt, G., 2005, Sierra Nevada EarthScope Project: International Federation of Digital Seismograph Networks, https://doi.org/10.7914/SN/XE_2005.
Pitt, A.M., Hill, D.P., Walter, S.W., and Johnson, M.J.S., 2002, Midcrustal, long-period earthquakes beneath northern California volcanic areas: Seismological Research Letters, v. 73, p. 144–152, https://doi.org/10.1785/gssrl.73.2.144.
Prodehl, C., 1979, Crustal structure of the Western United States: U.S. Geological Survey Professional Paper 1034, 74 p., https://doi.org/10.3133/pp1034.
Ruppert, S., Fliedner, M.M., and Zandt, G., 1998, Thin crust and active upper mantle beneath the southern Sierra Nevada in the western United States: Tectonophysics, v. 286, p. 237–252, https://doi.org/10.1016/S0040-1951(97)00268-0.
Ryall, A., and Ryall, F., 1983, Spasmodic tremor and possible magma injection in Long Valley caldera, eastern California: Science, v. 219, p. 1432–1433, https://doi.org/10.1126/science.219.4591.1432.
Saleeby, J., and Foster, Z., 2004, Topographic response to mantle lithosphere removal in the southern Sierra Nevada region, California: Geology, v. 32, p. 245–248, https://doi.org/10.1130/G19958.1.
Saleeby, J., Saleeby, Z., and Le Pourhiet, L., 2013, Epeirogenic transients related to mantle lithosphere removal in the southern Sierra Nevada region, California: Part II. Implications of rock uplift and basin subsidence relations: Geosphere, v. 9, p. 394–425, https://doi.org/10.1130/GES00816.1.
Savage, B., Ji, C., and Helmberger, D.V., 2003, Velocity variations in the uppermost mantle beneath the southern Sierra Nevada and Walker Lane: Journal of Geophysical Research, v. 108, 2325, https://doi.org/10.1029/2001JB001393.
Shelly, D.R., Hardebeck, J.L., Ellsworth, W.L., and Hill, D.P., 2016, A new strategy for earthquake focal mechanisms using waveform-correlation-derived relative polarities and cluster analysis: Application to the 2014 Long Valley Caldera earthquake swarm: Journal of Geophysical Research: Solid Earth, v. 121, p. 8622–8641, https://doi.org/10.1002/2016JB013437.
Smith, K.D., von Seggern, D.P., Blewitt, G., Preston, L., Anderson, J.G., Wernicke, B.P., and Davis, J.L., 2004, Evidence for deep magma injection beneath Lake Tahoe, Nevada-California: Science, v. 305, p. 1277–1280, https://doi.org/10.1126/science.1101304.
Smith, K.D., Kent, G.M., von Seggern, D.P., Driscoll, N.W., and Eisses, A., 2016, Evidence for Moho-lower crustal transition depth diking and rifting of the Sierra Nevada microplate: Geophysical Research Letters, v. 43, p. 10,738–10,744, https://doi.org/10.1002/2016GL070283.
Snoke, J.A., 2003, FOCMEC: FOCal MEChanism Determinations, *in* Lee, W.H.K., Kanamori, H., Jennings, P.C., and Kisslinger, C., eds., International Handbook of Earthquake and Engineering Seismology: Amsterdam, Academic, International Geophysics, v. 81, p. 1629–1630, https://doi.org/10.1016/S0074-6142(03)80291-7.
Sousa, F.J., Saleeby, J., Farley, K.A., Unruh, J.R., and Lloyd, M.K., 2017, The southern Sierra Nevada pediment, central California: Geosphere, v. 13, p. 82–101, https://doi.org/10.1130/GES01369.1.
Spieth, M.A., Hill, D.P., and Geller, R.J., 1981, Crustal structure in the northwestern foothills of the Sierra Nevada from seismic refraction experiments: Bulletin of the Seismological Society of America, v. 71, p. 1075–1087.
Thompson, G., and Reyes, C., 2018, GISMO—A seismic data analysis toolbox for MATLAB [software package, version 1.20b]: http://doi.org/10.5281/zenodo.1404723 (accessed July 2019).
Twiss, R.J., and Unruh, J.R., 1998, Analysis of fault slip inversions: Do they constrain stress or strain rate?: Journal of Geophysical Research, v. 103, p. 12,205–12,222, https://doi.org/10.1029/98JB00612.
Unruh, J., and Hauksson, E., 2009, Seismotectonics of an evolving intracontinental plate boundary, southeastern California, *in* Oldow, J.S., and Cashman, P.H., eds., Late Cenozoic Structure and Evolution of the Great Basin–Sierra Nevada Transition: Geological Society of America Special Paper 447, p. 351–372, https://doi.org/10.1130/2009.2447(16).
Unruh, J., Hauksson, E., and Jones, C.H., 2014, Internal deformation of the southern Sierra Nevada microplate associated with foundering lower lithosphere, California: Geosphere, v. 10, p. 107–128, https://doi.org/10.1130/GES00936.1.
von Seggern, D.H., Smith, K.D., and Preston, L.A., 2008, Seismic spatial-temporal character and effects of a deep (25–30 km) magma intrusion below north Lake Tahoe, California-Nevada: Bulletin of the Seismological Society of America, v. 98, p. 1508–1526, https://doi.org/10.1785/0120060240.
Wadati, K., 1933, On the travel time of earthquake waves, Part II: Geophysical Magazine, v. 7, p. 101–111.
Waldhauser, F., and Schaff, D.P., 2008, Large-scale relocation of two decades of Northern California seismicity using cross-correlation and double-difference methods: Journal of Geophysical Research, v. 113, B08311, https://doi.org/10.1029/2007jb005479.
Wang, Y., Forsyth, D.W., Rau, C.J., Carriero, N., Schmandt, B., Gaherty, J.B., and Savage, B., 2013, Fossil slabs attached to unsubducted fragments of the Farallon plate: Proceedings of the National Academy of Sciences of the United States of America, v. 110, p. 5342–5346, https://doi.org/10.1073/pnas.1214880110.
Wong, I.G., and Chapman, D.S., 1990, Deep intraplate earthquakes in the western United States and their relationship to lithospheric temperatures: Bulletin of the Seismological Society of America, v. 80, p. 589–599.
Wong, I.G., and Savage, W.U., 1983, Deep intraplate seismicity in the western Sierra Nevada, central California: Bulletin of the Seismological Society of America, v. 73, p. 797–812.
Zandt, G., 2003, The southern Sierra Nevada drip and the mantle wind direction beneath the southwestern United States: International Geology Review, v. 45, p. 213–224, https://doi.org/10.2747/0020-6814.45.3.213.
Zandt, G., Gilbert, H., Owens, T.J., Ducea, M., Saleeby, J., and Jones, C.H., 2004, Active foundering of a continental arc root beneath the southern Sierra Nevada in California: Nature, v. 431, p. 41–46, https://doi.org/10.1038/nature02847.
Zoback, M.D., and Zoback, M.L., 1980, State of stress in the conterminous United States: Journal of Geophysical Research, , v. 85, p. 6113–6156, https://doi.org/10.1029/JB085iB11p06113.
Zoback, M.L., 1992, First- and second-order patterns of stress in the lithosphere: The World Stress Map Project: Journal of Geophysical Research, v. 97, p. 11,703–11,728, https://doi.org/10.1029/92JB00132.